To the Graduate Council:

I am submitting herewith a thesis written by John Gregory Chambers entitled "Mineralogical and Petrographical Characterization of Lunar Mare Soils and Basalts for Resource Utilization". I have examined the final copy of this thesis for form and content and recommend that it be accepted in partial fulfillment of the requirements for the degree of Master of Science, with a major in Geology.

Lawrence A. Taylor

Lawrence A. Taylor, Major Professor

We have read this thesis
and recommend its acceptance:

Accepted for the Council:

Associate Vice Chancellor
and Dean of The Graduate School

# MINERALOGICAL AND PETROGRAPHICAL CHARACTERIZATION OF LUNAR MARE SOILS AND BASALTS FOR RESOURCE UTILIZATION

A Thesis

Presented for the

Master of Science

Degree

The University of Tennessee, Knoxville

John Gregory Chambers

May, 1995

# ACKNOWLEDGMENTS

I would like to thank sincerely my major professor and advisor, Dr. Lawrence A. Taylor, for his help and guidance during the last three years. I would also like to extend my appreciation to the other committee members, Dr. Harry Y. McSween, Dr. Theodore C. Labotka, and Dr. Craig Barnes for their thoughtful and helpful criticisms of my thesis. I would especially like to extend my appreciation to Mr. Allen Patchen for his help in obtaining all of the X-ray digital-imaging data presented in my thesis. Dr. David S. McKay and Ms. Susan Wentworth have helped me by providing critical reviews of portions of my thesis. The Lunar Sample Curatorial staff has been extremely efficient in their efforts of providing the necessary samples for this research project. Dr. Ralph Harvey has been gracious by allowing me to use his computer and printer for image enhancement.

I was fortunate to receive funding from the Tennessee Space Grant Consortium and the NASA Graduate Student Research Fellowship Program. These fellowships allowed me to concentrate on my research efforts.

All of my family have been very supportive during the past three years. My parents offered me encouragement and support during the difficult times. For that, I thank you all. I thank my son, Benjamin, for tolerating my busy schedule and intermittent absence during this project.

# ABSTRACT

Colonization of the Moon requires usage of the indigenous resources. Efficient utilization of these natural resources requires detailed knowledge of the concentration and distribution of the various minerals and glasses. In addition, extraction feasibility must be investigated. Application of X-ray digital-imaging techniques, previously and currently used to evaluate terrestrial mineral engineering problems, were applied to characterize the mineralogy and petrography of some lunar high-Ti mare basalts and soils. The results indicate that high-Ti immature and submature mare soils and high-Ti basalts contain similar amounts of ilmenite, contrary to previous evaluations. In addition, mineral liberation analyses show that the amounts of free ilmenite in the immature and submature soils and crushed basalts were similar. However, analysis of the magnetic separation of these basalts and soils shows that ilmenite from the basalts was enriched ~ 60% better than the ilmenite from the soils. This dichotomy is attributed to the presence of Fe-metal bearing impact-produced glass adhering to soil grains. Impact-produced melting caused the ilmenite content of mature soils to be considerably less, as compared to basalts and immature and submature soils with similar titanium content. The raw mare soils are excellent feedstocks for hydrogen reduction to produce an oxygen supply on the Moon, because the soils have similar ilmenite content as the basalts and they are already pulverized.

In addition to mineral resource evaluations, detailed soil modal data were generated by X-ray digital imaging analyses of a suite of mare soils from the Apollo 11,

12, 15, and 17 sampling sites. These data represent the first collection of estimates of the total mineral and glass content, including the phases in multimineralic particles, of soils from all Apollo mare sites. These type of data are requisite for accurate calibration of remote sensing techniques. Remote sensing analyses are used to glean information about the mineralogical and petrological character of the Moon and other airless bodies. As such, accurate calibrations with mineral compositional data are necessary for obtaining reliable modelling results by spectral reflectance studies.

# TABLE OF CONTENTS

PAGE


## PART 1: INTRODUCTION

1. Introduction....2

## PART 2: MINERAL LIBERATION AND BENEFICIATION OF LUNAR HIGH-TI MARE BASALT, 71055: DIGITAL-IMAGING ANALYSIS

1. Abstract....6
2. Introduction....6
3. Analytical Methods....8
4. Results and Discussion....10
5. Conclusions....25
6. References....26

## PART 3: QUANTITATIVE MINERALOGICAL CHARACTERIZATION OF LUNAR HIGH-TI MARE BASALTS AND SOILS FOR OXYGEN PRODUCTION

1. Abstract....28
2. Introduction....29
3. Analytical Methods....32
4. Results and Discussion....34
5. Conclusions....64
6. References....65

PAGE

**PART 4:** X-RAY DIGITAL-IMAGING OF LUNAR MARE SOILS: TRUE MODAL ANALYSES OF APOLLO 11, 12, 15, AND 17 SAMPLES

1. Abstract....71

2. Introduction....72

3. Analytical Methods....74

4. Lunar Soil Formation....76

5. Results and Discussion....80

6. Summary....98

7. References....100

VITA....104

# LIST OF TABLES

TABLE PAGE

## PART 2: MINERAL LIBERATION AND BENEFICIATION OF LUNAR HIGH-TI MARE BASALT, 71055: DIGITAL-IMAGING ANALYSIS

1. Size/shape information for ilmenite and plagioclase in 71055,74 high-Ti basalt thin section.....13

2. Summary of possible ilmenite feedstocks of 45-90 μm fraction produced from crushing and magnetic beneficiation of high-Ti basalt 71055.....24

## PART 3: QUANTITATIVE MINERALOGICAL CHARACTERIZATION OF LUNAR HIGH-TI MARE BASALTS AND SOILS FOR OXYGEN PRODUCTION

1. True modal data (volume %) for the 45-90 μm and 45-74 μm size fractions of crushed high-Ti mare basalts and high-Ti mare soils, respectively.....36

2. Ilmenite liberation and abundance in 45-74 and 45-90 μm bulk fractions of mare soils and crushed high-Ti basalts.....44

3. Ore grade, enrichment ratio (E.R.), and mass yield of magnetically generated ilmenite-rich feedstocks from the 45-74 and 45-90 μm fractions of the mare soils and basalts.....57

4. Oxygen yield predictions and feedstock tonnage for hydrogen reduction of various lunar materials.....61

## PART 4: X-RAY DIGITAL-IMAGING OF LUNAR MARE SOILS: TRUE MODAL ANALYSES OF APOLLO 11, 12, 15, AND 17 SAMPLES

1. Phase abundances of the soils (90-150 μm size fraction) characterized by this study. .....84

TABLE PAGE

2. Particle Petrography of the soils (90-150 μm size fraction) characterized by this study.....90

# LIST OF FIGURES

FIGURE PAGE

## PART 2: MINERAL LIBERATION AND BENEFICIATION OF LUNAR HIGH-TI MARE BASALT, 71055: DIGITAL-IMAGING ANALYSIS

1. Cumulative mineral fraction vs. crystal width (A), average diameter (B), aspect ratio (C),and form factor (D) for ilmenite and plagioclase grains in 71055,74.....11

2. 71055 pyroxene, plagioclase, and olivine compositions plotted as molar components: Di, Hd, En, and Fs for pyroxene; Fa and Fo for olivine; An and Ab for plagioclase.....13

3. Mineral Liberation graphs for ilmenite (A), plagioclase (B), and pyroxene (C) in the 45-90 μm fraction head sample of basalt 71055 .....15

4. Minimum-crush curve for ilmenite and plagioclase in basalt 71055 .....19

5. Modal mineralogy of head sample and various magnetic splits of the 45-90 μm fraction of crushed basalt 71055 .....22

## PART 3: QUANTITATIVE MINERALOGICAL CHARACTERIZATION OF LUNAR HIGH-TI MARE BASALTS AND SOILS FOR OXYGEN PRODUCTION

1. Mosaic of digitized BSE images from thin-sections of (A) basalt 71055 and (B) basalt 10058.....38

2. Representative digitized BSE images from grain mounts of the 45-74 μm size fractions of mare soils (A) 71061, (B) 71501, and (C) 10084 .....41

3. Minimum crush-size curves for ilmenite in mare basalt 71055 (fine-grain) and 10058 (medium-coarse grain) .....48

4. Representative digitized BSE images from grain mounts of the 45-90 μm size fractions of crushed mare basalts (A) 71055 and (B) 10058.....50

FIGURE PAGE

5. Schematic representation of the mineral liberation history of mare soils as a function of $I_s$/FeO (*i.e.*, surface exposure).....53

6. Ilmenite liberation curves for crushed mare basalts (45-90 μm) and mare soils (45-74 μm).....55

## **PART 4:** X-RAY DIGITAL-IMAGING OF LUNAR MARE SOILS: TRUE MODAL ANALYSES OF APOLLO 11, 12, 15, AND 17 SAMPLES

1. Schematic representation of the petrographic history of mare soils as a function of $I_s$/FeO (*i.e.*, surface exposure).....81

2. Variation of Al-rich glass (impact glass) content of mare soils versus $I_s$/FeO.....85

3. Variation of the normative/modal ilmenite ratios of mare soils of varying maturity .....87

4. Petrographic development of mare soils.....91

5. Ratio of modal mineral abundance (volume %) to particle count data (volume %)..94

6. Comparison of petrographic agglutinates versus Is/FeO data of mare soils (A-15 and A-17) from *Morris* [1976] compilation and data from this study.....96

# PART 1

# INTRODUCTION

# INTRODUCTION

Just as the early pioneers used the available resources to help establish permanent homes in the American frontier, explorers of the Moon and Mars must also use the indigenous resources in order to decrease the burden on the mother planet. It has been long realized that the deep gravity well of the Earth makes it difficult and expensive to transport building material, food, fuel, and oxygen to space. For the sake of efficiency, natural space resources must be converted into products to be used by a future lunar base.

Geological information enhances the mining and extraction of natural materials from a planet. For instance, consider the oil and gas exploration efforts on Earth. As compared to Earth, the Moon is a rather simple planetary body. Nevertheless, only a minor amount of lunar samples has been returned to the Earth for study, providing for limited geological control. These samples were collected from the two main geological provinces of the Moon: the light-colored, rugged highlands and the dark-colored, smooth maria. The highlands are principally composed of plagioclase-rich debris of plutonic rocks. Fe-rich basalts comprise most of the maria. No sample was taken from a bedrock outcrop during the Apollo missions. In fact, all samples were collected from a loosely consolidated mixture of rock, mineral, and glass fragments, termed the regolith. The lunar regolith was formed mainly by impacts of meteorites and micrometeorites. Its thickness is variable, ranging from 10-20 meters in the highlands to 3-5 meters in the maria. A detailed understanding of the nature of the lunar regolith

will greatly facilitate resource utilization efforts, especially during early missions when mining bedrock is probably not feasible.

One of the most sought after lunar commodities is an oxygen supply. A lunar liquid oxygen supply (LLOX) will be used for life-support systems and, most importantly, as an oxidant for rocket propulsion systems. Over twenty processes have been proposed to generate LLOX. *Taylor and Carrier* [1992] considered that reducing ilmenite with hydrogen gas was one of the most feasible processes. This is the only process in which experiments have been performed using actual lunar samples. Both lunar high-Ti basalts and soils (< 1 cm fraction of the regolith) have been used in these experiments. It is uncertain which is better to use for large-scale production of a LLOX supply.

In addition to collecting geological samples from a planet, much information can be gleaned by remote sensing efforts. Most of these techniques collect data from the outer surface of a body. Since all large, airless, rocky bodies, such as the Moon, likely possess impact-produced regoliths, remote sensing analyses of these objects generate compositional data about the regolith, not bedrock. Calibrating these data with the compositions of actual samples from the study area (*e.g.*, the Moon) quantifies modelling efforts. This provides yet another reason to study the lunar regolith.

In order to characterize quantitatively the mineral and glass content of the lunar soils and basalts, X-ray and backscattered electron (BSE) digital-imaging analyses have been performed with an Oxford Instruments energy dispersive spectrometer (EDS) mounted on a Cameca SX-50 electron microprobe (EMP) at the Department of

Geological Sciences, the University of Tennessee. The data are the basis of a three part thesis. The first part describes the results of crushing, sizing, and magnetic separation experiments with a high-Ti (ilmenite-rich) basalt. The ilmenite resources of high-Ti basalts and soils are discussed in the second part. The third part presents the first collection of modes of the total mineral and glass content, including those phases in multimineralic particles, of a suite of soils from all mare sites.

# PART 2

# MINERAL LIBERATION AND BENEFICIATION OF LUNAR HIGH-Ti MARE BASALT, 71055: DIGITAL-IMAGING ANALYSES

## ABSTRACT

Knowledge of the abundances of various lunar minerals and the ability to beneficiate effectively these minerals are important requirements for ultilization of lunar resources. SEM/EMP digital-imaging analyses of raw materials and beneficiated products provide an important step toward accurate mineral liberation estimates. Such analyses have shown that mineral liberation predictions made with width vs. mineral fraction curves are only approximate. Magnetic beneficiation of the 45-90 μm fraction of crushed high-Ti basalt, 71055 has concentrated ilmentite and plagioclase up to 70 volume % (79 weight %) and 95+ volume %, respectively. Comminution of basalt 71055 to < 90 μm should increase the current feedstock yield from 5.5 weight % to 10.2 weight %. Decreasing the grade to 65 weight % ilmenite should raise the feedstock yield to 9.6 weight %, but higher troilite abundance must be tolerated (up to 1.7 weight %).


## INTRODUCTION

The success of a lunar base will be largely dependent on how well the indigenous materials are utilized to provide many necessities, such as rocket propellant, water, and building materials [*e.g., Taylor*, 1990] and there has been much speculation on uses of lunar resources. Realistic evaluations of mineral abundances and of the ability to generate lunar mineral or glass feedstocks (concentrations of various components) are prerequisites for efficient exploitation of lunar resources. While the raw lunar regolith will be adequate for most bulk material needs, extraction of certain components will require the beneficiation of specific minerals and glasses, such as ilmenite, for $O_2$, $H_2$, $^3He$, Fe, and

Ti, agglutinates, for Fe, glass, and volatiles, volcanic glass, for $O_2$, glass, and volatiles, anorthite, for $O_2$, Al, and Si, and troilite, for S [*Taylor and Oder*, 1990].

Mineral beneficiation studies on Apollo 11, 16, and 17 lunar soils have shown that sizing and magnetic beneficiation can effectively concentrate various components [*Taylor and Oder*, 1990; *Oder and Taylor*, 1990]. In addition, *Taylor et al.* [1992] reported significant plagioclase and ilmenite concentration (*e.g.*, up to 98+ % plagioclase and 70 % ilmenite) upon crushing, sizing, and magnetic beneficiation of Apollo 11 and 17 lunar high-Ti basalts (10058 and 71055). Their work combined X-ray mapping and petrographic analyses to assess mineral liberation and concentration.

A major goal of any mineral resource endeavor is accurate mineral liberation predictions. Most operations rely on experience to estimate and characterize expected liberation of different raw materials. Reliable mineral liberation predictions are essential to a lunar mining project. Unfortunately, published descriptions of lunar basalts are largely semi-quantitative and do not provide much insight for predicting mineral liberation. However, SEM/EMP digital-imaging analyses provide a timely and accurate means of quantifying mineral morphology and size, and this is an important step toward quantification of mineral liberation appraisals. Therefore, automated SEM/EMP digital-imaging methods are being used in lunar resource characterization [*e.g., Heiken and Vaniman, 1990; Heiken et al., 1992; Taylor et al., 1993*].

Digital-imaging analyses of the minerals and textures of a rock (*i.e.*, in thin-sections) and crushed/beneficiated products (*i.e.*, grain mounts of sized and magnetically processed particles) permit evaluation of quantitative mineral liberation estimates [*e.g., Heiken and*

*Vaniman*, 1990]. This paper describes the observations of digital-imaging data collected from a thin-section and grain mounts (of beneficiated material) of ilmenite-rich, high-Ti basalt 71055. The grades and mass yields of various ilmenite feedstocks produced from 71055 are evaluated herein. In addition, the mineral associations of various magnetic splits are discussed.

## ANALYTICAL METHODS

The preparation of basalts 71055 was discussed by *Taylor et al.* [1992] and is reviewed herein. Rock chips of basalt 71055 were lightly crushed in a shatterbox, sieved into 90-150, 45-90, 20-45, and < 20 μm size fractions, and then magnetically separated with a Frantz Isodynamic Separator, which possessed instrumentation for both separation and magnetization measurements. Portions of each magnetic split were used to make polished grain mounts for petrographic examination. Mineral compostional data obtained with a Cameca SX-50 EMP at the University of Tennessee and data from *Dymek et al.* [1975] were used to characterize the phases in basalt 71055. The beam current, beam size, voltage, and counting times were 30 nA, 5 μm, 15 kV, and 20 seconds respectively. Both natural and synthetic standards were used for calibration. Quantitative EDS chemical analyses were performed on many (10 - 20) 100 % pyroxene fragments in various magnetic splits. The digital-imaging acquisition and processing were performed with an Oxford (Link) Instruments Energy Dispersive Systems (EDS) eXL II mounted on the Cameca SX-50. The Featurescan and Phase Distribution Analysis software program

permits user-defined chemical criteria for the identification of the various phases of a sample (*e.g.*, high Ca and Al and low Fe are indicative of plagioclase).

A modal analyses of 71055,74 was obtained by conventional point counting [*Taylor et al.*, 1992] and checked with the Oxford *Image-Phase Analysis* program. In addition, size and shape data were collected for plagioclase and ilmenite with the digital-image processing technique. The ophitic and interconnected nature of the pyroxene precluded accurate size/shape analyses, as the software cannot distinguish between grain boundaries of the same phase. The head sample (crushed and sized rock and mineral fragments not subjected to magnetic processing) of the 45-90 μm size fraction was analyzed with the Oxford Mineral Liberation program. Mineral liberation data of various magnetic splits of the 45-90 μm fraction are discussed, but space considerations permit only selected data to be presented.

At this point, it is important to review definitions used in digital-imaging morphology analyses. Size/shape parameters used in this paper are listed below.

**feret**- caliper measurements of a grain or particle;

**width** - smallest feret of a given grain;

**mean diameter**- average of all ferets of an object;

**aspect ratio**- length to width ratio; maximum to minimum feret ratio;

**form factor**- $(4\pi \text{ area})/(\text{perimeter}^2)$; a dimensionless value that describes circularity; a circle and square have values of 1 and 0.785, resp; form factor inversely correlates with surface area/volume ratios and shape factors.

**clean-** used in this study for clean mineral fragments to mean 80-100 % free of attached other phases;

## RESULTS AND DISCUSSION

### Traditional and Digital-imaging Petrography

Mineral textures, abundances, and chemistry of Apollo 17 high-Ti basalt 71055 have been described by *Dymek et al.* [1975] and *Taylor et al.* [1992]. 71055 is a fine-grained, vesicular, ophitic, ilmenite-rich basalt. Average grain size is about 0.5 mm. Modal mineralogy, determined by traditional point-counting, is 42% clinopyroxene, 29% plagioclase, 20% ilmenite (27 weight %), 3% olivine, and 5% cristobalite. Digital-imaging analysis determined similar values. Ulvöspinel, troilite, FeNi metal, apatite, and mesostasis collectively constitute < 5 volume % of 71055,74. Mineral association was variable, but a strong association of troilite and FeNi metal is obvious. Fe-rich pyroxene is commonly located next to cristobalite or mesostasis, a result of late-stage crystallization. Pyroxene occurs as radiating fan-shaped clusters (20-40 μm wide blades) and blocky equant grains (0.5-1.0 mm). Because of ophitic texture, much of the pyroxene is interconnected, which makes automated size measurements impossible. Plagioclase is present as laths (0.1-0.3 x 1-2mm) and interstitial patches. Ilmenite grains occur as skeletal blades with amoeboid rims (0.2-0.3 x 1-3 mm) and as discrete subhedral to euhedral crystals (0.1-0.4 mm).

Figure 1 graphically displays cumulative curves of the various size/shape parameters

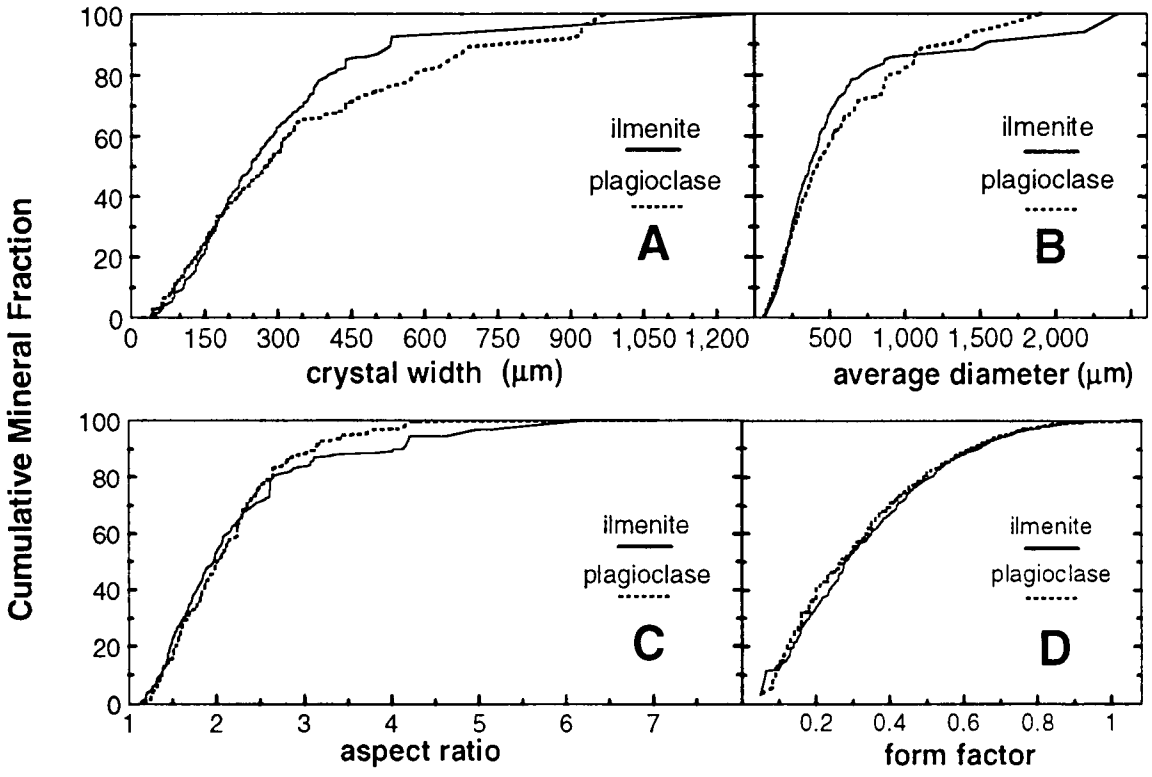



**Figure 1.** Cumulative mineral fraction vs. crystal width (A), average diameter (B), aspect ratio (C), and form factor (D) for ilmenite and plagioclase grains in 71055,74. Note that the vertical scale represents volume % .

used to characterize the ilmenite and plagioclase in 71055. Table 1 lists the averages, standard deviations, and ranges of various size/shape parameters of ilmenite and plagioclase.

## Mineral Chemistry

Understanding the mineral chemistry of a sample is a requirement for using phase identification software. Figure 2 displays the silicate mineral chemistry of basalt 71055. In addition, ilmenite was determined to contain 1-3 weight % MgO.

**Table 1.** Size/shape information for ilmenite and plagioclase in 71055,74 high-Ti basalt thin section. Data are from this study.

| **parameter** | **ilmenite** | **plag** | **parameter** | **ilmenite** | **plag** |
|---|---|---|---|---|---|
| **mean width**[†] | 132 | 117 | **mean aspect ratio**[§] | 1.93 | 2.05 |
| std. dev.(1σ) | 122 | 110 | std. dev.(1σ) | 0.63 | 0.65 |
| range | 22-1255 | 22-970 | range | 1.14-6.2 | 1.15-7.02 |
| **mean avg. diam**[†] | 199 | 180 | **mean form factor**[§] | 0.55 | 0.56 |
| std. dev.(1σ) | 190 | 170 | std. dev.(1σ) | 0.22 | 0.22 |
| range | 52-2410 | 52-1890 | range | 0.05-1 | 0.05-1 |

[†]micrometers ; [§]dimensionless

## Explanation of Mineral Liberation Graphs

The mineral liberation graphs used in this paper are complicated, but are extremely informative for liberation and beneficiation studies. As an illustration of this, we will discuss their usage and present the data for the 45-90 μm size fraction. This size fraction is the most effective for ilmenite beneficiation of this rock.

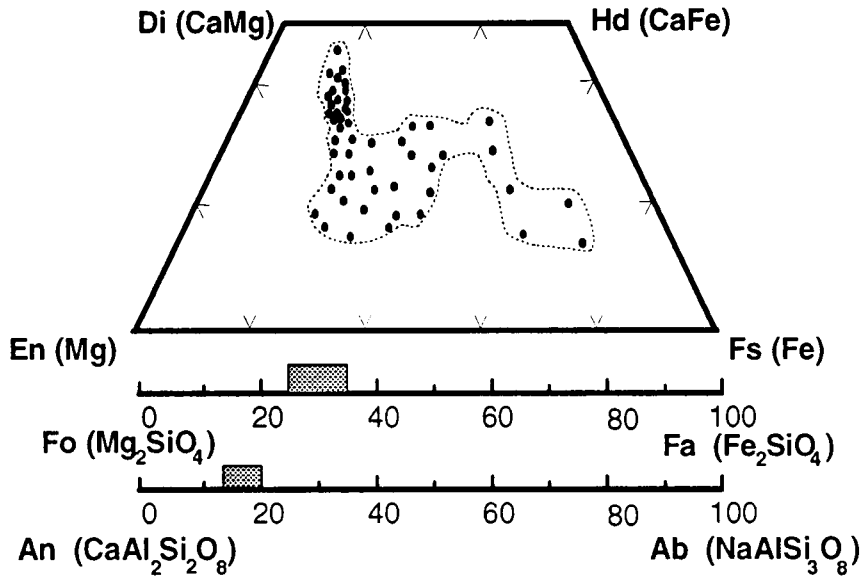


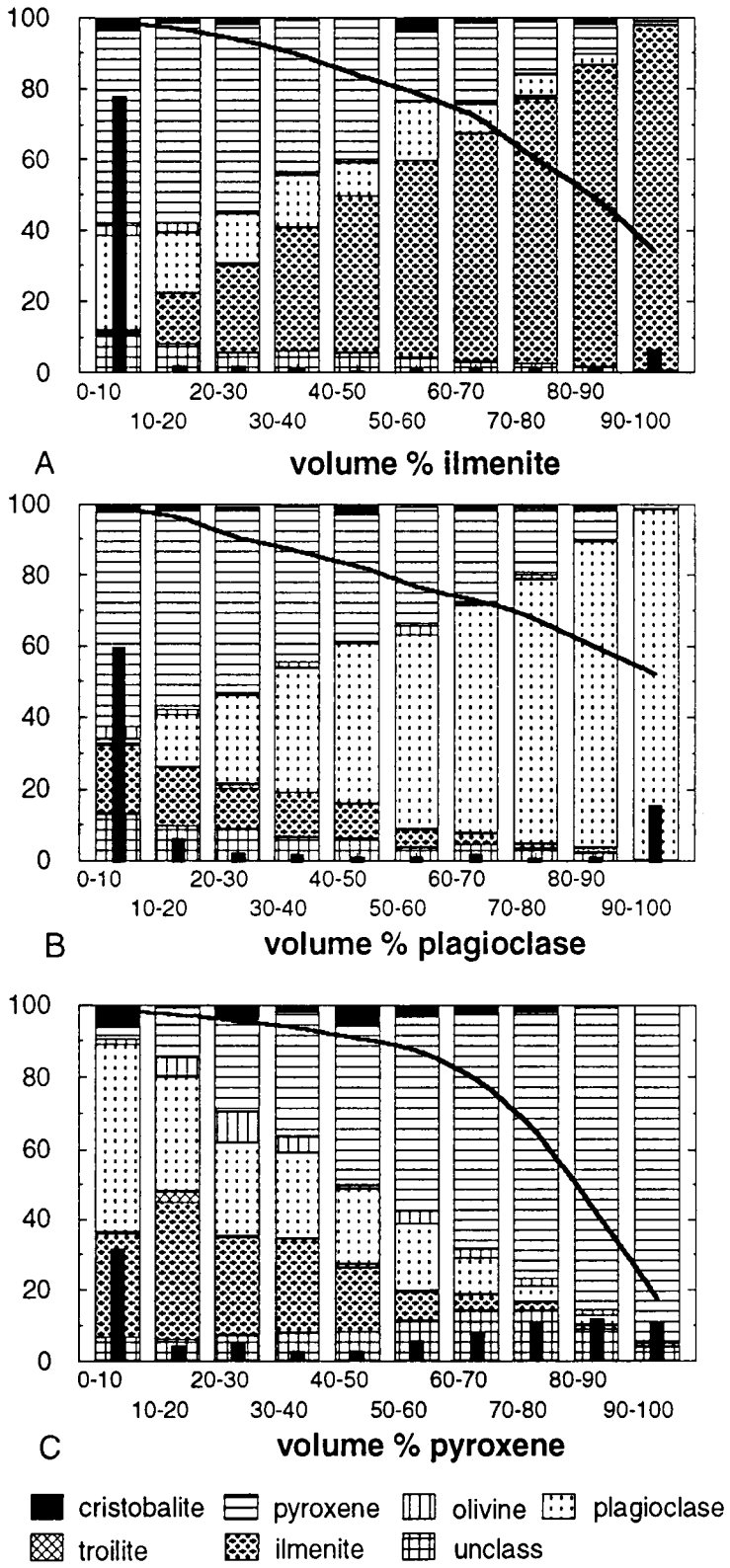

**Figure 2.** 71055 pyroxene, plagioclase, and olivine compositions plotted as molar components: Di, Hd, En, and Fs for pyroxene; Fa and Fo for olivine; An and Ab for plagioclase.

In Figure 3, the horizontal axes are divided into bins according to mineral volume percent. In essence, each bin represents particles (*i.e.*, mineral and rock fragments) that contain different amounts of a given mineral (*e.g.*, 0-10 % ilmenite, 10-20 % ilmenite, *etc.*). The bin values of the x-axes increase from left (*e.g.*, Figure 3A 0-10 % ilmenite) to right (*e.g.*, 90-100 % ilmenite). These patterned bars depict the average mineralogic makeup of particles containing a given volume % of the mineral listed on the horizontal axis (*e.g.*, ilmenite for Figure 3A); that is, they represent the mineral association for grains in that bin.

The narrow black bars, in Figure 3, depict the percentage of all particles that have various amounts of the x-axis mineral (*e.g.*, ilmenite for Figure 3A). For example, in Figure 3A, about 78 % of all particles have 0-10 % ilmenite. The significance of these bars is manifested in assessing the degree of mineral liberation that occurred upon the crushing of the rock. If crushing had completely liberated all the ilmenite, the particle % bars would show a bimodal distribution. In other words, only ilmenite-free and 100 % ilmenite particles would exist. However, inspection of these bars in Figure 3A shows that particles are present which cover the entire range of ilmenite concentrations. Therefore, crushing basalt 71055 to 90 μm did not completely liberate the ilmenite grains from the other minerals in the basalt.

The curves that traverse these graphs are cumulative mineral liberation curves for the 45-90 μm size fraction. They indicate the cumulative fraction of a mineral that is located in a bin and those bins to the right of it. For example, in Figure 3A the curve has a value of about 73 volume % ilmenite at the 60-70 % bin. This translates as 73 % of the ilmenite

**Figure 3.** Mineral Liberation graphs for ilmenite (A), plagioclase (B), and pyroxene (C) in the 45-90 μm fraction head sample of basalt 71055. Note that the vertical axes are scaled axes for all data on the graphs. The patterned bars, dark narrow bars, and curve show modal mineralogy, paticle %, and cumulative mineral %, respectively.


100
80
60
40
20
0
0-10
10-20
20-30
30-40
40-50
50-60
60-70
70-80
80-90
90-100
A
volume % ilmenite
B
volume % plagioclase
C
volume % pyroxene
cristobalite
pyroxene
olivine
plagioclase
troilite
ilmenite
unclass

in this grain mount (45-90 μm head sample) is present as particles which have at least 60 volume % ilmenite. Since these data are based on volume %, not particle %, they are invaluable to quantitative mineral liberation assessments.

In summary, Figures 3A-3C indicate that ilmenite, plagioclase, and pyroxene were not completely liberated upon crushing to 90 μm. That is, crushing basalt 71055 produced about 9 % clean ilmenite particles (clean = 80-100 %), 15 % clean plagioclase, 24 % clean pyroxene, and 51 % multimineralic particles in the 45-90 μm fraction. The mineral liberation curve shows that 50, 60, and 42 volume % of the ilmenite, plagioclase, and pyroxene, respectively, occur in clean mineral fragments.

## Mineral Liberation: Basalt

The degree of mineral liberation generated upon crushing controls the grade and yield of feedstock that can be produced by subsequent beneficiation processes (*e.g.*, magnetic separation). As the particle size decreases, the degree of liberation of the various phases increases. The crush-size necessary to generate clean (80-100 % free) mineral fragments from a rock is largely controlled by the size of the mineral grains in the rock [*e.g., Taylor et al.*, 1992]. Crushing coarse-grained rocks will produce more clean mineral fragments than crushing fine-grained rocks, for a given size fraction. Therefore, certain grain-size parameters of the minerals in the rock should be useful for estimating the degree of mineral liberation for various lunar basalts [*e.g., Heiken and Vaniman*, 1990].

Earlier attempts at quantifying terrestrial mineral liberation predictions have been mostly unsuccessful, but automated SEM/EMP techniques, such as used here, should

provide the key to more accurate assessments [*Wills*, 1992]. *Heiken and Vaniman* [1990] utilized automated SEM digital-imaging methods to generate cumulative ilmenite fraction vs. width curves (like Figure 1A) which they used to calculate minimum crush-size curves, and we have prepared similar curves for ilmenite and plagioclase in 71055 (Figure 4). The aspect ratios and shape factors (*i.e.*, 1/form factor) are important parameters that will affect the actual degree of liberation. Basically, as the form factor increases, the nature of the grain boundaries becomes more intricate (*i.e.*, like a jig-saw puzzle). As a mineral becomes less blocky, the form factor decreases and aspect ratio increases. Therefore, the width becomes a less accurate characterization of mineral liberation.

By comparing the grain size and shape data from the thin-section of basalt 71055 to the grain mounts of the head samples (Figure 3), we can judge the accuracy of mineral liberation predictions (based upon Figure 4). Specifically, Figure 4 shows that approximately 90 % of the ilmenite and plagioclase grains are greater than 100 μm wide. According to the principle stated by *Heiken and Vaniman* [1990], these curves suggest that crushing basalt 71055 to 90-100 μm should liberate about 90 % of the ilmenite and plagioclase. Therefore, mineral liberation data for the 45-90 μm size fraction head sample was examined to check the accuracy of this estimate. Figure 3 demonstrates that only 50 volume % of the ilmenite and 60 volume % of the plagioclase occur as clean (80-100 %) particles (in the 45-90 μm fraction). Furthermore, combination of the mineral liberation data for all < 90 μm head samples (*i.e.*, 20-44 μm; < 20 μm) indicates that only 62 volume % of the ilmenite and 66 volume % of the plagioclase are clean.

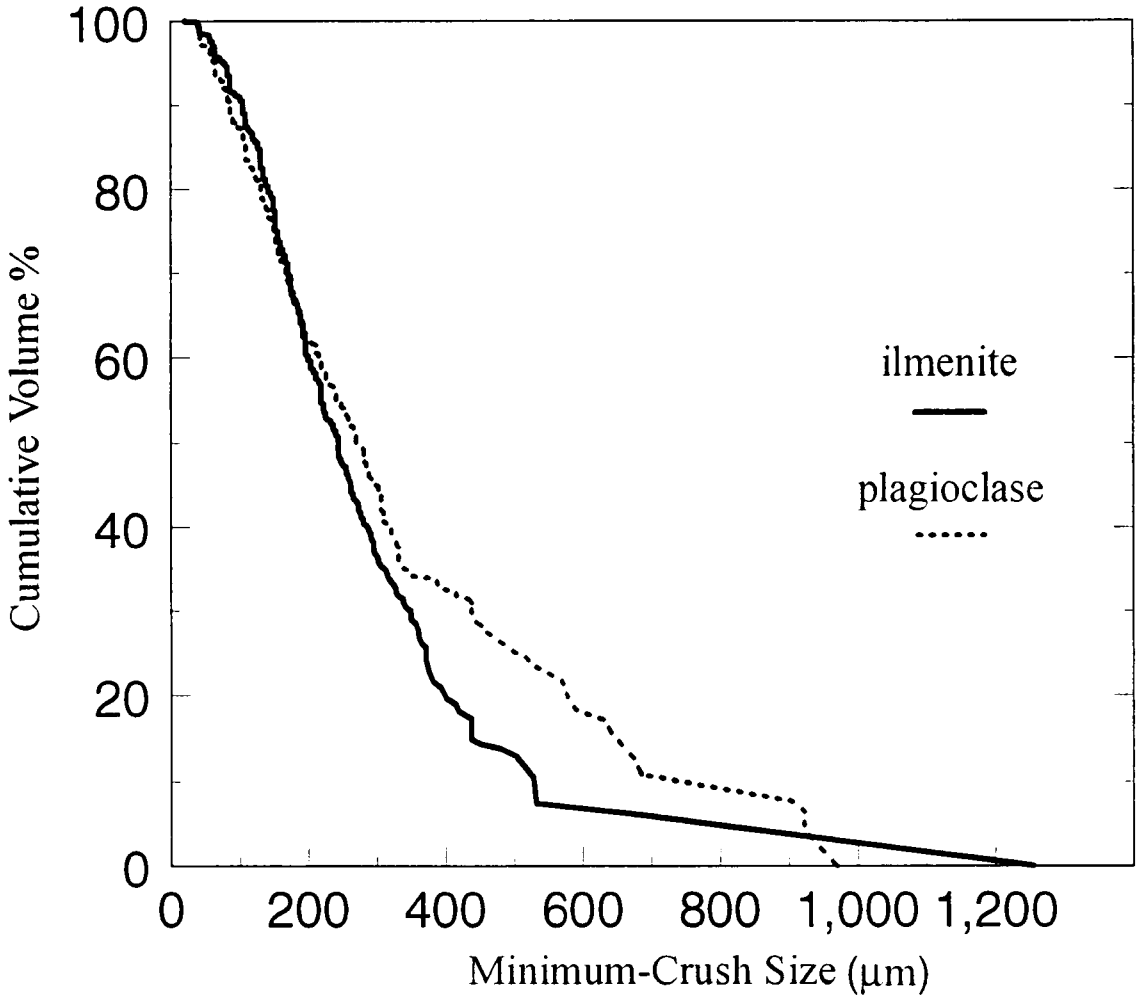



**Figure 4**. Minimum-crush curve for ilmenite and plagioclase in basalt 71055. Similar curves were presented by *Heiken and Vaniman* [1990] in order to estimate the amount of free ilmenite fragments produced upon crushing to a given size fraction.

Predicted total liberation was not obtained. However, the prediction scheme of *Heiken and Vaniman* [1990] will only apply to minerals with minimum aspect ratios and maximum form factors. With rock 71055, intricate grain shapes of ilmenite and plagioclase greatly affected mineral liberation. However, it is difficult to quantitatively determine which shape parameter had the most control on liberation. *Heiken and Vaniman* [1990] showed that for ilmenite, in four A-17 high-Ti basalts, there was no apparent correlation between the shape parameters and grain size. Therefore, it is impossible to generally state that the large or small mineral grains have undesirable shapes. It is likely that an empirical correction factor could be determined (by a series of liberation studies) that would provide more accurate liberation estimates.

Another factor that is difficult to predict is the crushability of a rock. Minerals frequently crush differently such that some may have a tendency to concentrate in the finer grain-size fractions. In addition, it is generally known that mineral cleavage affects liberation. This is demonstrated here by better liberation of plagioclase than ilmenite, although ilmenite had a larger average grain size (Table 1).

## Mineralogy of Magnetic Splits

Different minerals have different magnetic susceptibilities [*e.g., Carmichael*, 1982]. The use of magnetic separation techniques for lunar ilmenite beneficiation schemes has been demonstrated by previous lunar sample studies [*e.g., Taylor and Oder*, 1992; *Oder and Taylor*, 1992]. The details of the magnetic separation techniques used here are given in *Oder and Taylor*, [1990]. *Taylor et al.* [1992] described the modal mineralogy and

petrography of some of the various magnetic susceptibility splits made from processing crushed basalt 71055. Figure 5 is a combined modal mineralogy diagram and a magnetogram of the 45-90 μm size fraction of the crushed basalt, 71055. The patterned bars show the modal mineralogy of the head sample and each magnetic split, and the curve displays the weight % (mass yield) of each magnetic split (*i.e.*, of the total rock mass). As expected, plagioclase was efficiently concentrated in the lowest magnetic split (95+ volume % plagioclase). While significant pyroxene abundances are present in all splits > 3 μcc/g , it is mostly concentrated in the 14-41μcc/g split (75 volume %). This split comprises 17.6 weight % of the whole rock. Ilmenite was concentrated up to 70 volume % (79 weight %) in the 50-93 μcc/g split and also was significantly concentrated in the two highest magnetic splits. Note that the 50-93 μcc/g split is 5.5 weight % of the initial rock mass. Troilite is concentrated in the highest magnetic split, and this is partially due to the common ferromagnetic FeNi metal association. As expected, FeNi metal abundance is highest in the most magnetic split. However, the abundances of FeNi metal, apatite, and mestostasis are too low to be displayed.

## Distribution of Pyroxene and Ilmenite in Various Magnetic Splits

The magnetic susceptibility of a particle is a function of mineral association, mineral chemistry, size, and shape [*e.g., Carmichael*, 1982]. Figure 5 shows that pyroxene and ilmenite are distributed over a range of magnetic susceptibilities (14-50 to > 239 μcc/g). Furthermore, mineral liberation data (not provided herein) show that at least 5-10 % of these particles in each magnetic split are 90-100 % free pyroxene and ilmenite. Chemical analyses of 100 % free pyroxene fragments from various magnetic fractions indicates that

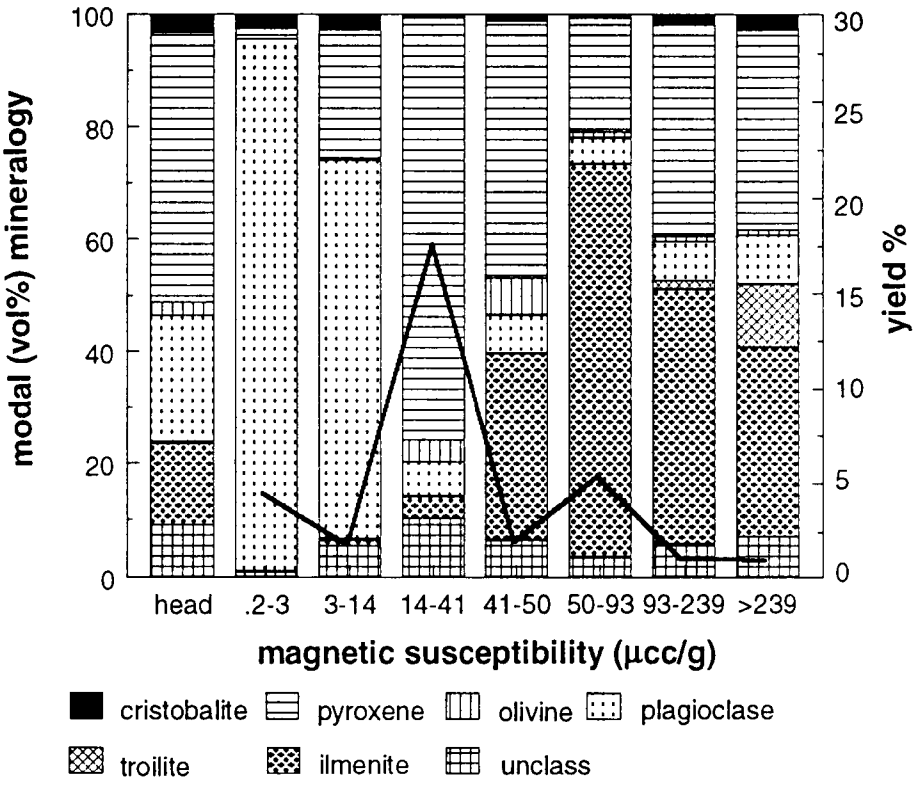



**Figure 5.** Modal mineralogy of head sample and various magnetic splits of the 45-90 μm fraction of crushed basalt 71055. The curve shows the wt% of each split (of the total rock). Note that the vertical axes are scaled differently; the left is for the modal data and the right is for the yield % of each magnetic split.

no systematic chemical variation in FeO content exists. In addition, the small chemical variation of ilmenite suggests that chemical factors are not strongly affecting its magnetic susceptibility.

Small amounts of minor, attached, high-magnetic susceptibility phases can influence separation efficiency. Petrographic examination of various grains mounts indicated that troilite grains with FeNi blebs (1-5 μm) are attached to numermous pyroxene and ilmenite particles. Furthermore, mineral association data reveal that the amount of troilite attached to 90-100 % pyroxene and ilmenite particles increases from 0 % (14-41 μcc/g) to 0.4 and 0.7 % (>239 μcc/g). In addition, the widths of the attached troilite grains increase in the higher magnetic susceptibility splits, from about 2 to 30 μm, in the four higher magnetic splits. Collectively, these data demonstrate that minor amounts of attached troilite and FeNi metal decreased the efficiency of magnetic separation of pyroxene and ilmenite. However, Figure 5 shows that the combined mass of the two most magnetic splits is < 2 weight % of the whole rock, indicating that this is not a major concern to large scale mining operations.

## Ilmenite Feedstock Mass Yields

Although mineral concentration (*i.e.*, ore grade) is important to any mining operation, mass yields are of ultimate significance. Figure 5 indicates that ilmenite was concentrated at 70 volume % (79 weight %) in the 50-93 μcc/g split of the 45-90 μm size fraction. However, the mass yield was only 5.5 weight % of the total rock mass, crushed to 150 μm (Table 2). In order to increase the mass yield, it is necessary to consider lesser

grades for the ilmenite feedstock by combining several of the higher magnetic splits. In fact, if all magnetic splits greater than 41 μcc/g, of this size fraction, are combined, the mass yield of feedstock will increase from 5.5 to 9.6 weight %, while the ore grade only decreases from 79 to 65 weight % ilmenite. However, troilite increases from 0.2 to 1.7 weight %, and this could prove deleterious to ilmenite reduction processes to produce oxygen because sulfuric acid will likely be created [*Taylor and Carrier*, 1992].

**Table 2**. Summary of possible ilmenite feedstocks of 45-90 μm fraction produced from crushing and magnetic beneficiation of high-Ti basalt 71055.

| | 50-93 μcc/g | | | >41 μcc/g | | |
|---|---|---|---|---|---|---|
| **crush-size** | **grade**[†] | **yield**[§] | **troilite**[‡] | **grade** | **yield** | **troilite** |
| < 150 μm | 79 | 5.5 | 0.2 | 65 | 9.6 | 1.7 |
| < 90 μm | 79 | 10.2 | 0.2 | 65 | 17.8 | 1.7 |

[†]weight % ilmenite; [§]weight % of total crushed rock; [‡]weight %

Enhanced ilmenite liberation can significantly increase feedstock mass yield. This can be achieved by mining only coarse-grained basalts or by further grinding of fine-grained basalts (*e.g.*, 71055). In fact, the 45-90 μm fraction is only 34 weight % of the crushed basalt, and the 90-150 μm material is 46 weight %. Further comminution of the 90-150 μm fraction could effectively double the mass yield (5.5 to 10.2 weight %) of the 79 weight % ilmenite split in the 45-90 μm fraction. Combining further grinding with lower grade (65 weight % ilmenite) should increase the ulitimate mass yield to 17.8

weight %. In addition we have not even considered the < 45 μm size fractions which can yield significant quantities of clean mineral fragments, but are more difficult to beneficiate effectively.

## CONCLUSIONS

Digital-image analyses of thin sections of lunar basalts produce a quantification of size/shape parameters of the major minerals. These data provide mineral liberation predictions. However, this study demonstrates that minimum crush-size curves (such as those used by *Heiken and Vaniman*, 1990) provide only a rough first approximation of ilmenite and plagioclase liberation for basalt 71055 (< 100 μm = 90 % liberated ilmenite vs. 62 % in practice). This is probably due to the shape of the ilmenite and plagioclase grains in the rock. Mineral liberation data and petrographic examination of various magnetic separates indicates that attached troilite with FeNi blebs prevented better ilmenite beneficiation (> 79 weight %). This study has shown that crushing, sizing, and crude magnetic beneficiation of basalt 71055 has concentrated ilmenite up to 70 volume % (79 weight %), but the yield of the feedstock was only 5.5 weight %. Further comminution of the 90-150 μm material should increase the yield to 10.2 weight %. A lower ore grade (65 weight % as compared to 79 weight % ilmenite) will provide a significant increase in feedstock yield (5.5 to 9.6 weight %), but higher troilite concentration must be tolerated (0.2 to 1.7 weight %).

# REFERENCES


Carmichael, R.S., Magnetic Properties of Minerals and Rocks. In the *Handbook of Physical Properties of Rocks*, CRC Press, Boca Raton, 230-287, 1982.

Dymek, R.F., A.L. Albee, and A.A. Chodos, Comparative Mineralogy and Petrology of Apollo 17 Mare Basalts: Samples 70215, 71055, 74255, 75055, *Proc. Lunar Sci. Conf. VI*, 49-77, 1975.

Heiken, G.H. and D.T. Vaniman, Characterization of Lunar Ilmenite Resources, *Proc. Lunar Planet. Sci. Conf. XX*, 239-247, 1990.

Heiken, G.H., D.T. Vaniman, and H. Hawkins, Sulfur as a Lunar Resource, In *Engineering, Construction, and Operations in Space III*, Amercian Society of Civil Engineers, New York, 555-564, 1992.

Oder, R.R., and L.A. Taylor, Magnetic Beneficiation of Highland and Hi-Ti Mare Soils: Magnet Requirements, In *Engineering, Construction, and Operations in Space II*, 133-142, 1990.

Taylor, L.A., Rocks and Minerals in the Regolith of the Moon: Resources for a Lunar Base, In *Advanced Materials--Applications Mining and Metal Process*. Prin., Lakshmanan (ed.), SME, 29-47, 1990.

Taylor, L.A. and R.R. Oder, Magnetic Beneficiation of Highland and Hi-Ti Mare Soils: Rock, Mineral, and Glassy Components, In *Engineering, Construction, and Operations in Space III*, 143-152, 1992.

Taylor, L.A., D.S. McKay, J.Graf, A. Patchen, S. Wentworth, R.R. Oder, and E.A. Jerde, Magnetic Beneficiation of High-Ti Mare Basalts: Petrographic Analyses, *Lunar and Planet. Sci. Conf. XXIII*, 1415-16, 1992.

Taylor L.A. and D. Carrier, Production of Oxygen on the Moon: Which Prcesses are Best and Why, *AAIA Jour.*, v. 30, no. 12, p. 2858-63, 1992.

Taylor, L.A., J.G. Chambers, A. Patchen, E.A. Jerde, D.S. McKay, J. Graf, and R.R. Oder, Evaluation of Lunar Rocks and Soils for Resource Utilization: Detailed Image Analysis of Raw Material and Beneficiated Products, *Lunar and Planet. Sci. Conf. XXIV*, 1409-10, 1993.

Wills, B.A., Mineral Processing Technology, 5th Edition, Oxford, Pergamon Press, 855, 1992.

# PART 3

# QUANTITATIVE MINERALOGICAL CHARACTERIZATION OF LUNAR HIGH -Ti MARE BASALTS AND SOILS FOR OXYGEN PRODUCTION

# ABSTRACT

Efficient lunar resource utilization requires accurate and quantitative evaluation of mineral and glass abundances, distribution, and extraction feasibility, especially for ilmenite. With this in mind, true modal analyses were performed on high-Ti mare basalts and soils with X-ray/BSE digital-imaging techniques, and these data indicate that: **1)** Ilmenite concentrations are similar for basalts and immature to submature soils with similar $TiO_2$ content; **2)** Ilmenite liberation of crushed mare basalts and immature-submature mare soils are comparable (*i.e.*, both contain similar amounts of free ilmenite); **3)** Because of the impact-melting and agglutination of primary minerals, mature mare soils contain less ilmenite (both free and attached). Modal analyses of magnetic separates of high-Ti mare basalts and soils show that: **1)** Ilmenite was concentrated by a factor of $\geq 3.3$; **2)** Soil ilmenite was concentrated to factors of 1.7-2.3. The lower soil ilmenite separation efficiency is attributed to Fe°-bearing agglutinitic glass and amorphous rinds adhered to soil particles. Mass yields of magnetically generated feedstocks were generally less than 5 weight % in most cases. Calculation of oxygen yield (as released by hydrogen gas reduction of ilmenite) shows that: **1)** Beneficiated basalt will provide the most oxygen (8-10 %), due to higher ilmenite concentration; **2)** Reduction of raw immature-submature mare soils and basalts will produce similar amounts of lunar liquid oxygen (LLOX) (2.1-3.1%); **3)** Raw Fe-rich pyroclastic soil, 74220, will provide more oxygen (5.4%) than beneficiated high-Ti mare soils and half that of beneficiated high-Ti mare basalts. High-Ti mare soils are

attractive resources for LLOX production due to their unconsolidated nature, high ilmenite abundance, and widespread occurrence. Energy-intensive excavation and comminution likely prohibits the basalt mining during early lunar occupation. Orange soils are important resources for LLOX and various volatile elements, but slower reaction rates and glass sintering pose potential difficulties for large-scale operations.

## INTRODUCTION

Colonization efforts require the usage of indigenous resouces. A lunar base will undoubtedly use the local rocks, minerals, and soils for construction materials and various chemical and metallurgical commodities. The raw lunar regolith will suffice for most bulk material needs such as radiation shielding [*Taylor and Oder*, 1990], but generation of certain products such as lunar liquid oxygen (LLOX), $H_2O$, S, Fe, Ti, Al, Si, and various gases may require mineral beneficiation of lunar rocks and soils. Resource characterization is a requisite for efficient utilization and must include data about mineral and glass abundance, distribution, and extraction from actual lunar samples.

One of the most important lunar commodities is oxygen. LLOX has obvious uses as fuel oxidant and for life-support. Although oxygen is virtually absent as a gaseous species on the moon (atmosphere ~ $10^{-12}$-$10^{-14}$ torr), the crustal rocks contain about 43 weight % oxygen in the form of silicate and oxide minerals. While over twenty processes have been proposed to generate LLOX from lunar resources, reduction of ilmenite with hot (900-1100 C°) hydrogen gas is considered one the most feasible

[*Taylor and Carrier*, 1992]. In addition, experimental data exist about the kinetics and oxygen yields of hydrogen reduction of ilmenite-rich lunar rocks and soils [*Gibson et al.*, 1994a,b; *Allen et al.*, 1994a,b,c]. However, the nature of lunar feedstock, mare rocks versus soils, is unresolved.

There has been much debate over whether to use mare soils or basalts as raw materials for mineral extraction, especially ilmenite [*Heiken and Vaniman*, 1990; *Vaniman and Heiken*, 1990; *DeLa'O et al.*, 1990; *Taylor and McKay*, 1992; *Taylor et al.*, 1992]. Ilmenite abundance in mare basalts and soils is an important issue in this controversy; the contrasting methods of petrographical descriptions of basalts and soils have contributed significantly to the uncertainity. Specifically, basalt ilmenite concentrations are reported as modes or modal percents, which is the actual abundance of ilmenite expressed either as volume or weight percentages [*Bates and Jackson*, 1990]. A modal analysis is performed by point-counting a representative cross-section of the sample (usually a thin-section) and assuming that areal fraction is equivalent to volume fraction. In contrast, petrographic characterizations of lunar soils are determined by particle-counting of grain mounts, with the tacit assumption that particle percent equals volume percent and modal percent.

It is not strictly correct to report soil particle counts as the soil modal composition. Particle counts include detailed information about the abundance of mineral fragments, various rock fragments, impact glasses, and glass-bonded aggregrates (*e.g.*, agglutinates); but these analyses do not determine true mineral areal percent (*i.e.*, modes), as mineral grains locked in rock fragments and fused-soil-particles

are not counted. These mineral grains can significantly add to the total mineral concentration value. For example, preliminary results reported by *Chambers et al.* [1994b] indicated that only about half the ilmenite is liberated (present as free grains) in the 45-74 μm fractions of various high-Ti mare soils. Therefore, with the standard particle-count data, it is not possible to compare quantitatively the mineral concentrations of lunar rocks and soils. It is imperative that true modal analyses be performed on lunar soils. In has been shown that X-ray digital-image analysis of soils and rocks provides accurate modal as well as particle-count data, allowing valid comparison of mineral content [*Chambers et al.*, 1994b; *Higgins et al.*, 1994a].

Mineral beneficiation of lunar rocks and soils based upon magnetic separation experiments provides an important data base for resource evaluation. Specifically, mineral beneficiation experiments with Apollo 11, 16, and 17 soils have determined that sizing and magnetic treatment can effectively concentrate various minerals and particles (*e.g.*, agglutinates) of lunar soils [*Taylor and Oder*, 1990; *Oder and Taylor*, 1990]. Similar beneficiation experiments with Apollo 11 and 17 high-Ti mare basalts have demonstrated even greater mineral concentrations [*Taylor et al.*, 1992]. Nevertheless, it is difficult to compare these data for basalt versus soil beneficiation, since petrographic characterizations were performed by the different methods described above.

This paper describes new mineralogical data obtained from raw and beneficiated samples previously studied by *Taylor and Oder* [1990] and *Taylor et al.* [1992]. Specifically, the new data consist of accurate modal and mineral distribution information obtained by X-ray digital-imaging analyses. The power of this technique is

obvious when considering its extensive application to terrestrial mineral engineering problems [*e.g., Petruk,* 1988a,b; *Sutherland and Gottlieb,* 1991]. Moreover, several efforts have shown that BSE/X-ray digital-imaging analyses are precise and quantitatively adequate for petrographic characterization of lunar rocks and soils [*Heiken and Vaniman,* 1990; *Heiken et al.,* 1992; *Taylor et al.,* 1993; *Chambers et al.,* 1994a,b; *Higgins et al.*, 1994]

## ANALYTICAL METHODS

Sample preparation was described by *Taylor and Oder* [1990] and *Taylor et al.* [1992] and is reviewed herein. Rock chips of lunar basalts 71055 and 10058 were lightly crushed in a shatterbox with a tungsten carbide swing mill and sieved into 90-150, 45-90, 20-44, and < 20 μm size fractions. Mare soils 71061, 71501, and 10084 were sieved into 74-150, 45-74, 20-44, and < 20 μm fractions. Magnetic beneficiation was performed with a calibrated Frantz Isodynamic Separator, which possessed instrumentation for both separation and magnetization measurements. Portions of each magnetic split and bulk size fraction were used to make polished grain mounts for optical petrographic examination and X-ray mapping.

Phase abundance and distribution analyses (by X-ray digital-imaging) of rocks and soils require the operator to know the minerals present in a sample. Therefore, detailed optical petrographic characterization was performed prior to X-ray mapping. The mineral abundance and association data of the grain mounts were obtained with an Oxford Instruments (LINK) Energy Dispersive Spectrometer (EDS) eXL II mounted on

a Cameca SX-50 EMP at the Dept. of Geological Sciences, the University of Tennessee. Backscattered electron (BSE) signals were used to discriminate between epoxy and grains. Phases were identified by characteristic X-ray spectrometry with the Oxford EDS. Specifically, the Oxford software, Featurescan and Phase Distribution Analysis (formerly Mineral Liberation), uses operator-defined chemical criteria to distinguish the various phases of a sample (*e.g.*, high Ca and Al and low Fe and Mg are indicative of plagioclase). Lunar glasses such as Ti-rich glass (~ 7-10 % $TiO_2$) and Al-rich glass (~10-20 % $Al_2O_3$) are treated as discrete phases, although their definitions are somewhat subjective and arbitrary. A full explanation of the chemical criteria used for phase indentification is given by *Higgins et al.* [1995]. The excitation potential, beam current, spot size, magnification, and counting times for phase identification were 20 kV, 3 nA, 1 μm, 135X, and 40 ms, respectively. For image analysis, the pixel, stepping, and image sizes were 1 μm, 4 μm, and 512 X 512, respectively. Mineral liberation results were generated from phase abundance data and digitized grain-images by *Phase Distribution Analysis*. At least 1000 particles were analyzed from each grain mount as per the criteria of *Sutherland and Gottlieb* [1991].

BSE digital-imaging was performed on polished thin-sections of high-Ti mare basalts 71055 and 10058. Ilmenite was discriminated from silicates, sulfides, and Fe-metal by BSE signal intensity. The excitation potential, beam current, and magnification for these analyses were 20 kV, 5nA, and 50X, respectively. The pixel and image sizes were 11 μm and 512 X 512. *Featurescan* was used to measure the

width, aspect ratio (length/width), and area of each ilmenite grain in the thin-sections. 1355 and 433 ilmenite crystals were analyzed from 71055 and 10058, respectively.

Chemical data for 45-74 μm size fractions of mare soil, used for normative calculations, were taken from unpublished analyses of *Taylor and Oder* [1990]. Whole-rock chemistry and whole-rock modal data of mare basalt 71055 were obtained from *Neal and Taylor* [1993].

Grain-size fractions ranging from 40-100 μm are well suited for beneficiation studies because coarser material generally does not have adequate mineral liberation and extremely fine material (< 40 μm) does not magnetically separate well [*Wills*, 1992; *Taylor and Oder*, 1990]. Unfortunately, the crushed rocks and soils were sieved into slightly different size fractions, but it is probably valid to compare the 45-90 and 45-74 μm fractions of the basalts and soils, respectively. Therefore, this paper concentrates on ilmenite liberation and beneficiation of these size fractions in comparing rocks and soils and in discussing feedstocks in general.

## RESULTS AND DISCUSSION

### Sample Mineralogy and Petrography

Five lunar samples were characterized during this project. Two of the samples are high-Ti mare basalts with distinctly different textures. These samples were chosen to evaluate the effect of grain size and shape on mineral liberation and beneficiation. The ferromagnetic intensity parameter, $I_s$/FeO, increases with maturity and is considered a generally-applicable surface-exposure index [*Morris*, 1976; *Morris*, 1978].

Using published $I_s$/FeO values as a guide, three high-Ti mare soils spanning a large range of maturity ($I_s$/FeO = 14-78) were chosen for study in order to quantify the degree of mineral liberation achieved naturally during regolith formation.

Soil minerals and glasses (as defined by this study and *Higgins et al.* [1995]) include pyroxene (clinopyroxne + orthopyroxene), plagioclase, olivine, ilmenite, Ti-rich glass (7-10 % $TiO_2$), Al-rich glass (10-20 % $Al_2O_3$), Fe-Mg-rich glass (pyroxene-like composition), apatite (all P-rich minerals are grouped as apatite), troilite (all S-rich minerals are grouped as troilite), Cr-rich spinel, K-rich mesostasis, native Fe metal, and cristobalite. Ti-rich glass is generally equivalent to volcanic basaltic glass (*e.g.*, 74220) and is a major constituent of pyroclastic beads in lunar soils. Al-rich glass is impact-generated glass, and it mainly occurs in agglutinates, melt-rocks, and soil breccia. The rock and soil modal data reported in Table 1 were acquired by X-ray digital-imaging analyses. It is important to emphasize that these data are true modes (actual volume percentages) not particle percentages of mineral fragments, as traditionally reported [*e.g.*, *Heiken and McKay*, 1974]. Because digital-imaging data were obtained for both basalts and soils, it is possible and valid to compare directly their mineral content. Agglutinate abundances are from unpublished data generated during the work of *Taylor and Oder* [1990]. All modal data for rocks and soils are reported in Table 1.

**Mare Basalt 71055**

Apollo 17 rock 71055 is a fine-grained, holocrystalline, vesicular, ophitic, high-Ti mare basalt. Pyroxene occurs as both equant grains (0.5-1.0 mm) and as blades (20-

**Table 1.** True modal data (volume %) for the 45-90 μm and 45-74 μm size fractions of crushed high-Ti mare basalts and high-Ti mare soils, respectively. Data collected by X-ray digital-imaging analyses of polished grain mounts.

| | basalts | | soils | | |
|---|---|---|---|---|---|
| **phase** | **71055** fine-grain | **10058** med-grain | **71061** $I_s$/FeO=14 | **71501** $I_s$/FeO=35 | **10084** $I_s$/FeO=78 |
| ilmenite | 16.7 | 12.8 | 11.2 | 13.7 | 6.7 |
| pyroxene | 51.5 | 49.3 | 32.3 | 34.8 | 33.3 |
| plagioclase | 25.8 | 32.3 | 14.8 | 15.9 | 16.2 |
| olivine | 1.5 | 0.0 | 4.7 | 5.8 | 1.3 |
| cristobalite | 2.5 | 2.8 | 0.6 | 0.5 | 0.4 |
| Cr-spinel | tr[§] | tr | 0.2 | 0.1 | 0.2 |
| troilite | 0.4 | 0.7 | 0.2 | 0.1 | 0.1 |
| Fe-metal | tr | tr | tr | 0.1 | 0.1 |
| apatite | 0.3 | 0.0 | tr | tr | 0.0 |
| K-rich glass | 0.3 | 0.9 | 0.6 | 0.4 | 0.0 |
| Al-rich glass[†] | - | - | 12.2 | 13.7 | 27.6 |
| Ti-rich glass[†] | - | - | 18.5 | 10.3 | 6.2 |
| FeMg-rich glass[†] | - | - | 4.3 | 4.2 | 5.5 |
| unclassified[‡] | 1.0 | 1.2 | 0.2 | 0.4 | 1.5 |

[§]tr = trace amounts, i.e., < 0.1 %

[†]Phases inherent to soils due to impact processes and pyroclastic glass mixing.

[‡]Unclassified refers to "phases" that did not meet the user-defined chemical criteria in *Phase Distribution Analysis*. This is mainly due to sampling phase boundaries and does not correspond to real undefined phases.

40 μm wide) growing as radial, fan-shaped clusters, intergrown with plagioclase. Plagioclase generally occurs both as laths (0.1-0.3 x 1-2 mm) and interstitial patches(0.3-0.8 mm across). Ilmenite grains occur as dendritic blades with amoeboid rims (0.2-0.3 x 1-3 mm) and as discrete subhedral to euhedral crystals (0.1-0.4 mm). Olivine is generally occluded by pyroxene. Cristobalite exists as irregular patches up to 0.2 mm in diameter. Troilite is anhedral (50-100 μm) and usually has native Fe inclusions (1-5 μm). Figure 1A is a mosaic of digitized BSE images from 71055 and displays the petrographic texture. Note the fine-grained nature and the intricate grain boundaries of ilmenite.

**Mare Basalt 10058**

Apollo 11 rock 10058 is a medium-grained, holocrystalline, ophitic, high-Ti mare basalt. Pyroxene is anhedral and equant, usually 1.0-1.5 mm across. Plagioclase occurs as laths ranging in length from 0.2 to 1mm, with aspect ratios of 3-5. Plagioclase glomerocrysts also occur. Ilmenite occurs as blades, often skeletal, (0.2-0.6 x 1-2 mm) and equant subhedral to euhedral crystals (0.5-0.8 mm). Cristobalite has a crackly texture. and it occurs interstitially and as patches. Native Fe metal is a common inclusion in cristobalite. Figure 1B, a mosaic of digitized BSE images, shows the texture of this basalt. Note the contrasting differences between 71055 and 10058 (Figure 1A and 1B).

**Mare Soil 71061**

Apollo 17 soil 71061 is an immature ($I_s$/FeO = 14) high-Ti mare soil [*Heiken and McKay*, 1974]. It is mainly composed of comminuted pyroxene, plagioclase,

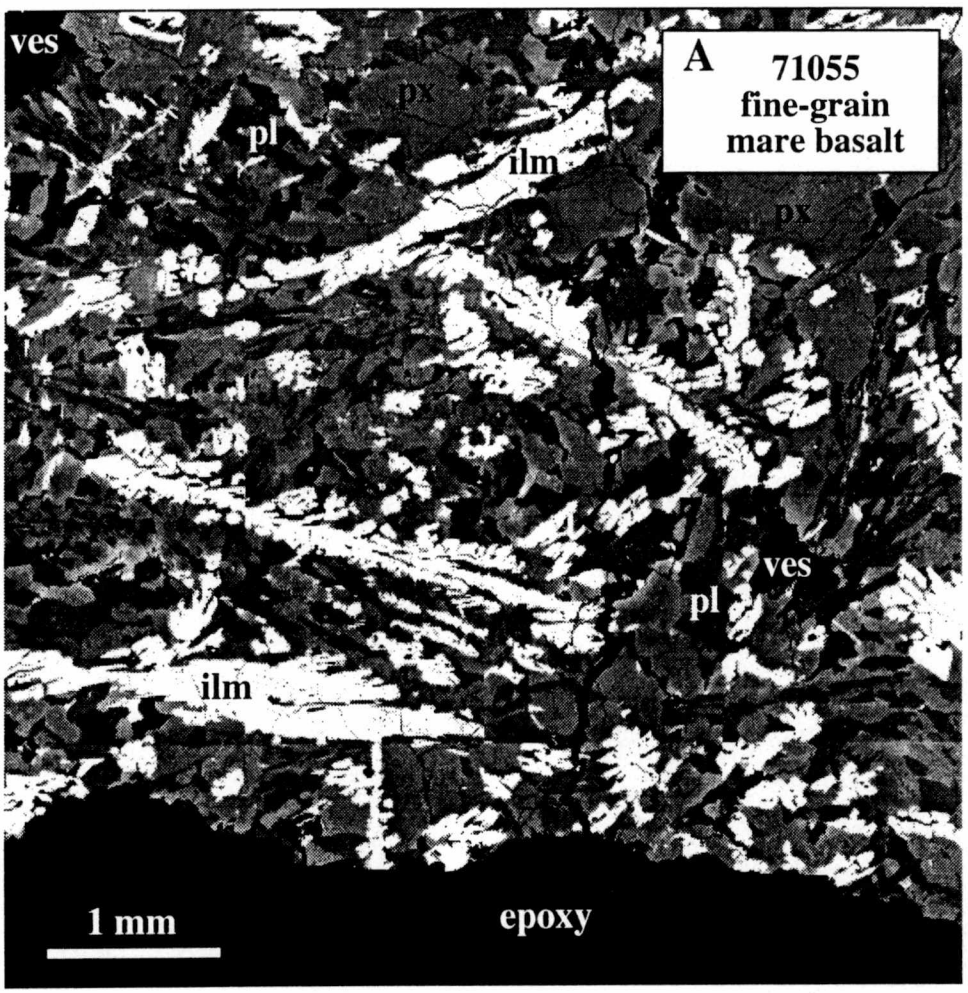



**Figure 1**. Mosaic of digitized BSE images from thin-sections of (**A**) basalt 71055 and (**B**) basalt 10058. The phases can be distinguished from relative differences in gray-level intensity. Key: **ilm** = ilmenite (white), **px** = pyroxene (medium to light gray), **pl** = plagioclase (dark gray), **crist** = cristobalite (very dark gray), and epoxy/vesicles (**ves**) are black. Minor phases such as Fe-metal and troilite are too small to discriminate from these images.

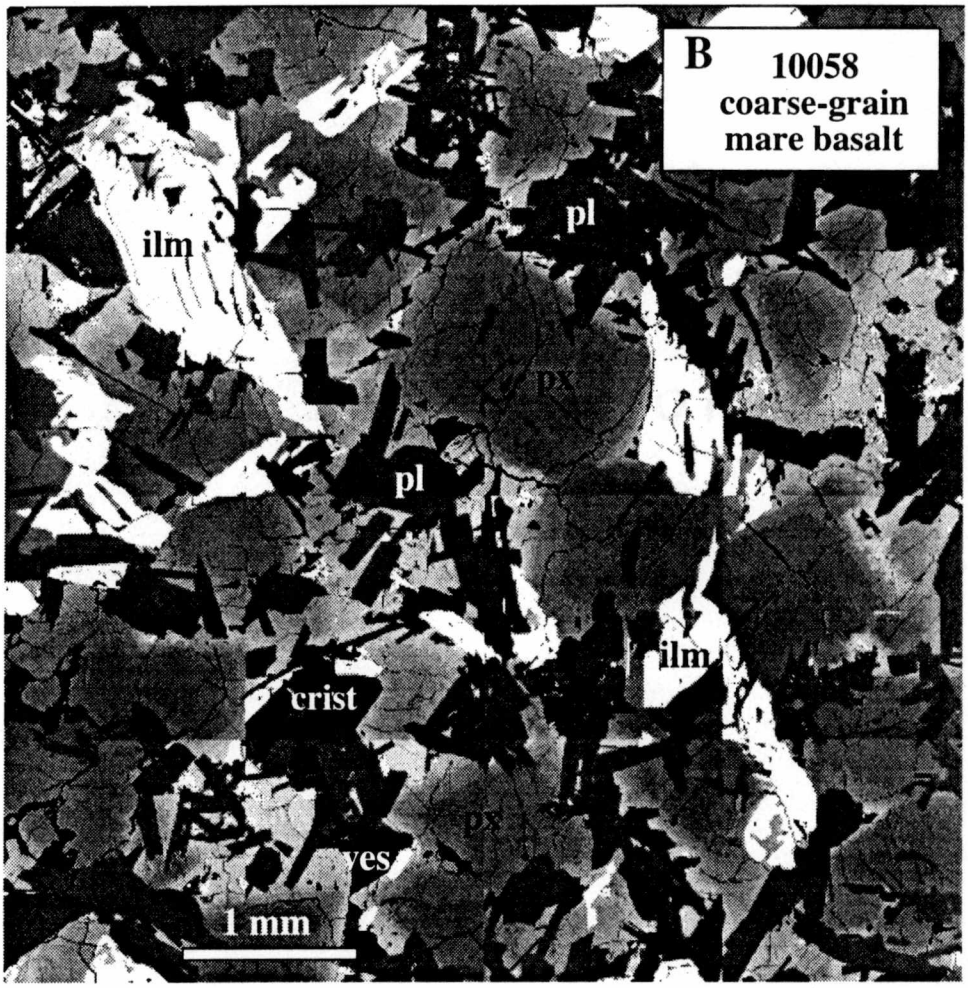



**Figure 1 (B).**

ilmenite, and basalt fragments. Ti-rich pyroclastic glass beads are common. Fused-soil components, such as breccia, melt rocks, and agglutinates are minor constituents[*Heiken and McKay*, 1974]. For instance, 71061 only contains 7% agglutinates in the 45-74 μm fraction [unpublished data from the work of *Taylor and Oder*, 1990]. The mean grain size of all soil material < 1 cm is 169.6 μm [*McKay, et al.*, 1974]. Figures 2A-2C are digitized BSE images from the polished grain mounts of all three mare soils.

**Mare Soil 71501**

Apollo 17 soil 71501 is a submature ($I_s$/FeO = 35) high-Ti mare soil with 26% agglutinates in the 45-74 μm fraction [*Heiken and McKay*, 1974; unpublished data from *Taylor and Oder*, 1990]. It it mainly composed of pyroxene, plagioclase, ilmenite, basalt fragments, and agglutinates. Pyroclastic glass beads are present, but minor. The mean grain size of the bulk soil (< 1 cm) is 82.5 μm [*McKay et al.*, 1974]. See figure 2B.

**Mare Soil 10084**

Apollo 11 soil 10084 is a mature ($I_s$/FeO = 78) high-Ti mare soil with 34% agglutinates in the 45-74 μm size fraction [*e.g.*, *Simon et al.*, 1981; unpublished data from *Taylor and Oder*, 1990]. This soil is mainly composed of pyroxene, plagioclase, ilmenite, basalt fragments, glassy breccia, and agglutinates. It has the highest Al-rich glass (impact-produced) content of the soils studied herein (Table 1). The mean grain size, as reported by *Duke et al.* [1970], is 84.5 μm. See figure 2C.

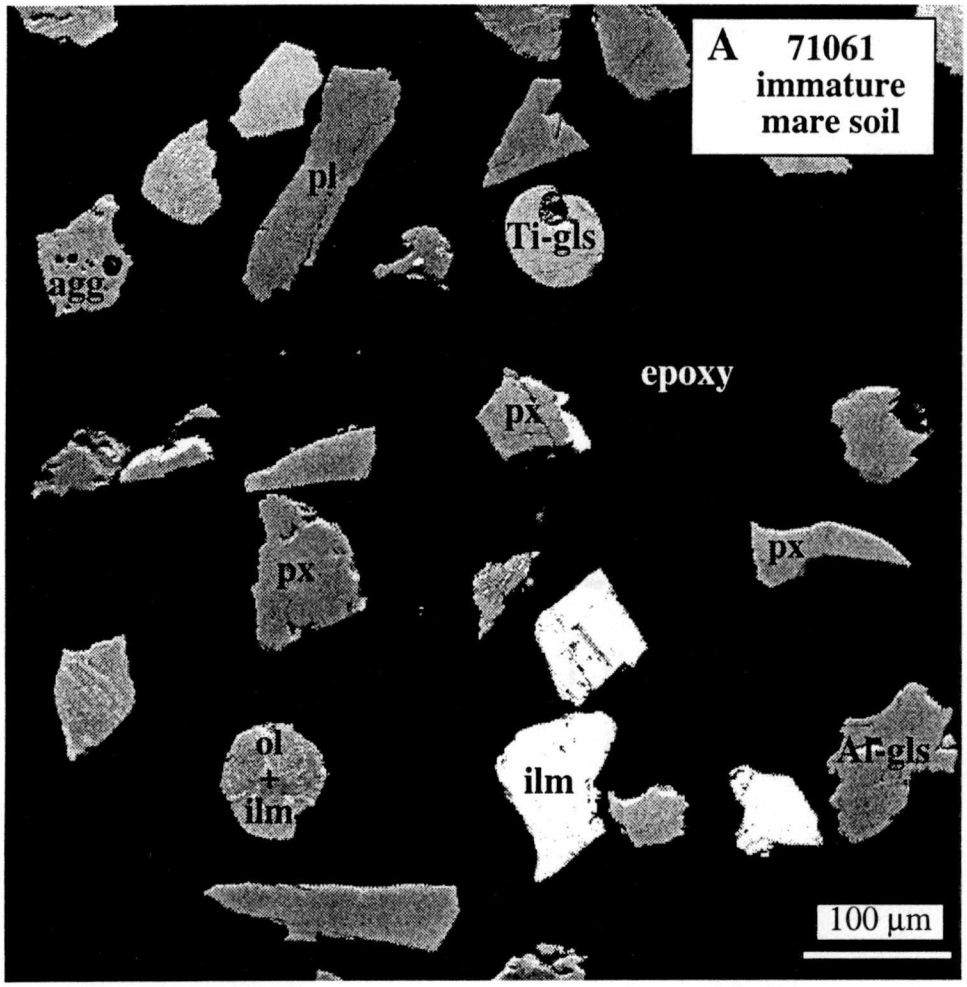



**Figure 2**. Representative digitized BSE images from grain mounts of the 45-74 µm size fractions of mare soils, (**A**) 71061, (**B**) 71501, and (**C**) 10084. Key: **ilm** = ilmenite (white), **px** = pyroxene (light gray), **pl** = plagioclase (medium gray), **agg** = agglutinate, **Ti-gls** = Ti-rich glass, and **Al-gls** = Al-rich glass (medium to dark gray).

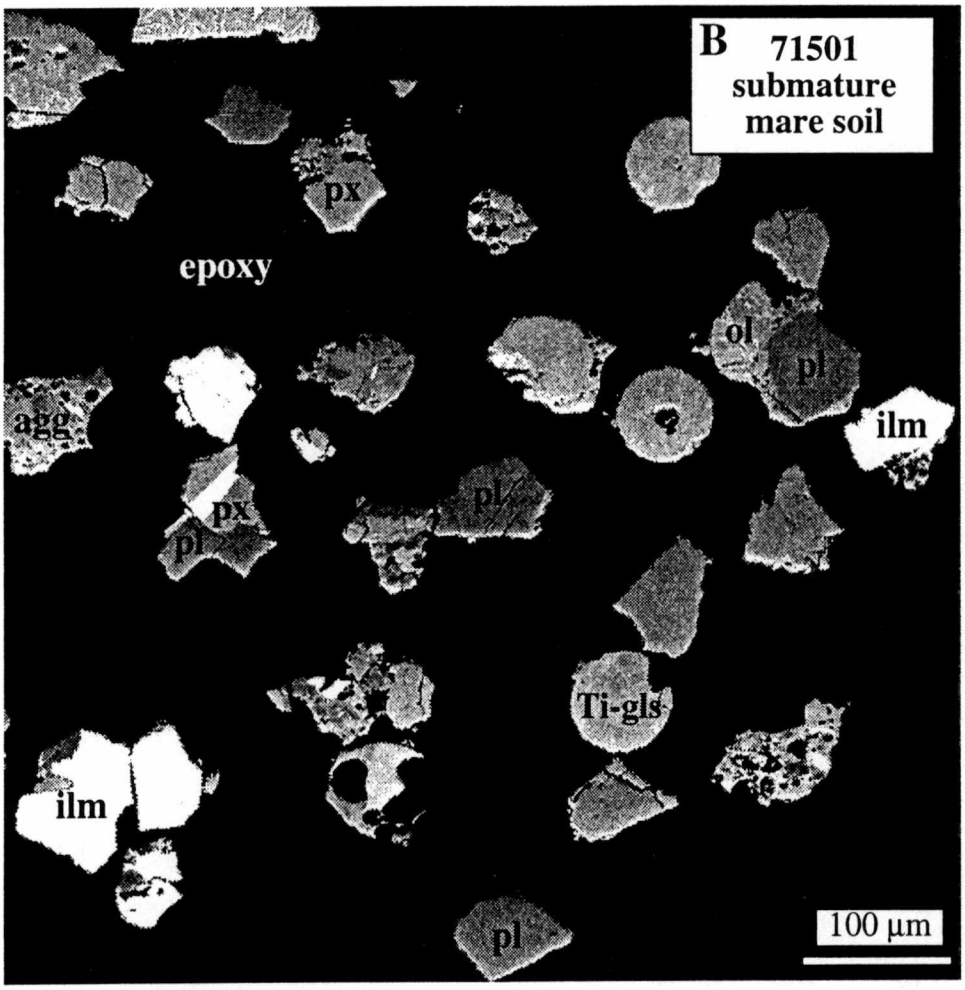

B 71501
submature
mare soil
px
epoxy
ol
pl
ilm
agg
px
pl
pl
Ti-gls
ilm
pl
100 µm

**Figure 2 (B).**

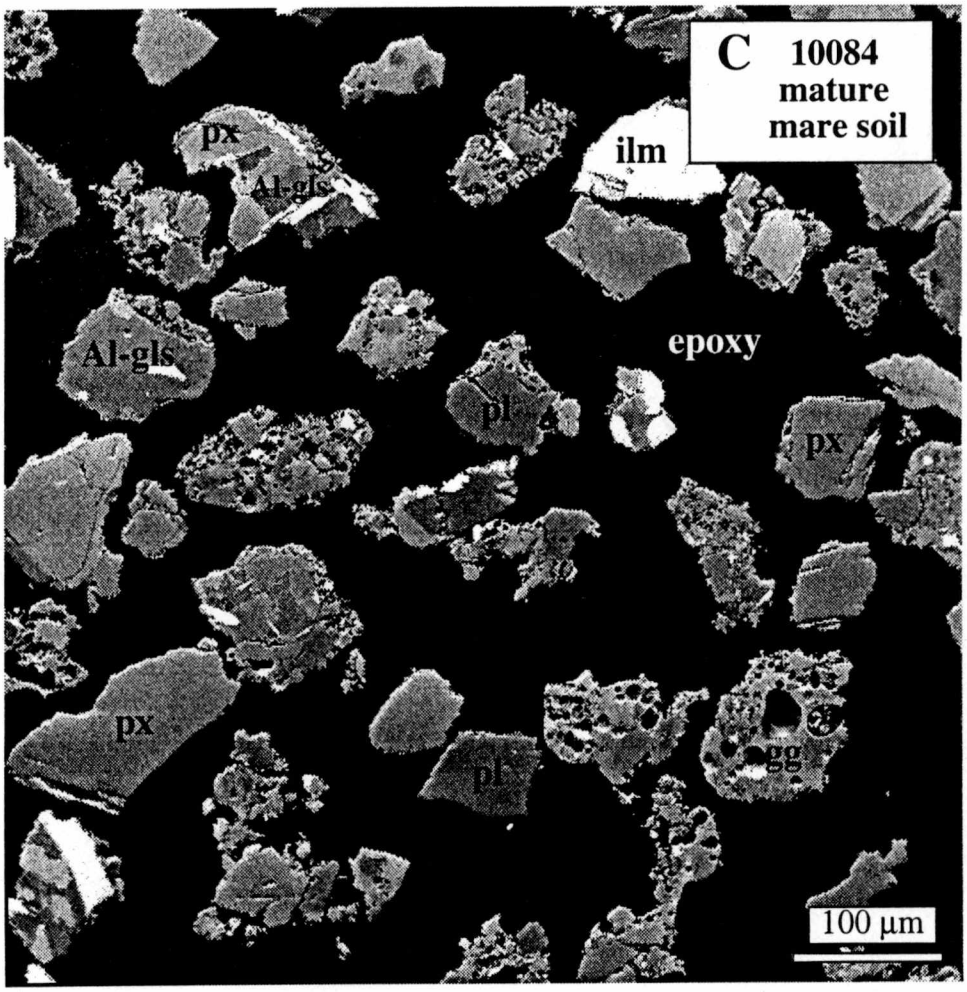

C 10084
mature
mare soil
px
ilm
Al-gls
Al-gls
epoxy
pl
px
px
pl
gg
100 µm

**Figure 2 (C).**

## Ilmenite Abundance: Mare Basalt vs. Soil

Given a mare basalt and a soil both with the same $TiO_2$ content, the rock will generally contain more ilmenite, especially for a mature soil. This is due entirely to the impact-produced melting which occurs during regolith formation [*Taylor and Oder*, 1990]. Although the difference in the ilmenite abundance is not large, traditional soil "modal petrology" incorrectly indicates that the lunar regolith contains exceedlingly small amounts of ilmenite. Our ilmenite modal data are summarized in Table 2 and demonstrate that ilmenite abundances of the basalts and immature-submature soils are similar. All samples have similar $TiO_2$ concentrations, and $TiO_2$ weight % largely controls the amount of ilmenite crystallized from basaltic magma.

**Table 2.** Ilmenite liberation and abundance in 45-74 and 45-90 μm bulk fractions of mare soils and crushed high-Ti basalts. $TiO_2$ content is provided for reference.

| sample | vol.% ilmenite | wt.% ilmenite[†] | degree of liberation[‡] | $TiO_2$ |
|---|---|---|---|---|
| **basalt** | | | | |
| 71055 (fine-grain) | 16.7 | 23.4 | 50 | 13.5 |
| 10058 (med-grain) | 12.8 | 18.5 | 78 | 10.1 |
| **soil** | | | | |
| 71061 ($I_s$/FeO=14) | 11.2 | 16.3 | 62 | 8.97 |
| 71501 ($I_s$/FeO=35) | 13.7 | 19.6 | 58 | 10.1 |
| 10084 ($I_s$/FeO=78) | 6.7 | 10.2 | 37 | 7.99 |

[†]Weight percentage data are calculated from volume percentage data using appropriate specific gravity values of all phases [*Johnson and Olhoeft*, 1982].
[‡]Degree of liberation = volume fraction of ilmenite that is 80-100% free.

As discussed above, mature soils are depleted in ilmenite as compared to basalts and fresh soils of comparable bulk chemistry. This is due to the formation of impact glass at the expense of primary minerals. The mineralogical effect of soil fusion is exemplified by comparing normative ("norm") and modal mineral abundances [*e.g.*, *Taylor and Oder*, 1990]. A normative calculation is the theoretical mineral content calculated from bulk chemistry and mineral formulae. The norms and modes of holocrystalline lunar basalts correspond closely for minerals exhibiting limited variance from ideal composition (*e.g.*, ilmenite and plagioclase). For example, the calculated and analyzed ilmenite concentrations of basalt 71055 are 25.7 and 26.3 weight %, respectively (norm/mode ratio = 0.98). In most cases, basalt whole-rock chemistry accurately predicts ilmenite adundance. The chemistry of soil does not change significantly with maturation, but the mineral content alters drastically, causing the norm/mode ratio to increase. For instance, the calculated and analyzed values of ilmenite for immature soil 71061 are 17.1 and 16.3 % (norm/mode = 1.05). In contrast, the normative and modal ilmenite for mature soil 10084 are 15.2 and 10 % (norm/mode = 1.52). This shows that bulk chemical data of mature soils relay marginally useful information about mineral abundances; therefore, modal analyses are required to determine ilmenite concentration.

In addition to volume percentage modes, determined by digital-imaging analyses, Table 2 contains ilmenite weight percentages as well. Weight percentage modes facilitate quantitative ilmenite resource evaluation due to large density differences of oxides and silicates. Weight percent data in Table 2 were converted

from volume percentage using appropriate specific gravity values of the various phases. The density of lunar glass is partially a function of chemistry, especially FeO concentration [*Frondel et al.*, 1970]. Mare agglutinitic glass (our Al-rich glass) is chemically similar to basalt [*Hu and Taylor*, 1977; *Walker and Papike*, 1981]; therefore, it has a density of ~ 2.75 g/cm$^3$ [*Johnson and Olhoeft*, 1982.]. Ti-rich and Fe-Mg-rich glasses (as described herein) generally contain more FeO than typical mare agglutinitic glass, and therefore they are denser (G ~ 3.0-3.25 [*Frondel et al.*, 1970]). A conservative value of 3.0 g/cm$^3$ was used for the specific gravities of these phases. Note the large increase of ilmenite abundance upon the weight percent conversion (Table 2).

## Mineral Liberation of Comminuted Basalts

Concentrating a specific mineral from basalt or soil requires adequate liberation of the ore mineral from the gangue minerals. In this case, it is desirable to have a low amount of silicate gangue material (*e.g.*, plagioclase, pyroxene, and various glasses) attached to ilmenite ore. The grade of a feedstock is the ore mineral weight percentage, in this case ilmenite weight percentage. The mass yield of a feedstock is the weight fraction (usually expressed as a percentage) of total starting rock or soil mass. The degree of liberation affects the grade and mass yield of feedstock produced by magnetic separation, since multimineralic particles have mixed susceptibilities.

Ore mineral size, shape, cleavage, crushability, and association determine the degree of liberation achieved by rock comminution. Therefore, large (0.5-1 mm),

blocky ilmenite crystals will be well liberated upon crushing high-Ti mare basalts. With this in mind, *Heiken and Vaniman* [1990] provided ilmenite width vs. ilmenite volume % percent curves ("minimum crush-size curves") for lunar basalts, regolith breccias, and orange soil. According to *Heiken and Vaniman* [1990], these curves predict the amount of free ilmenite released by crushing to a specific grain size. Experimental work shows that these curves do not predict exact ilmenite liberation, especially for basalts with complex ilmenite morphology [*Chambers et al.*, 1994a]. However, when comparing basalts with similar ilmenite shapes, they should indicate which are better for ilmenite extraction. High-Ti mare soils must be evaluated by X-ray digital imaging to determine quantitatively the degree of mineral liberation generated by meteorite bombardment.

The two lunar basalts discussed herein are excellent examples of how grain size and shape effect mineral liberation. As noted earlier, 71055 is a fine-grained basalt with dendritic and equant ilmenite crystals, and 10058 is a medium-grained basalt with equant and bladed ilmenite. Therefore, better mineral liberation is expected by crushing 10058. Using digitized BSE images, like Figure 1, ilmenite minimum-crush size curves (similar to those of *Heiken and Vaniman* [1990]) were calculated for the two basalts (Figure 3). These curves indicate that 85% and 94% of ilmenite in 71055 and 10058, respectively, is > 100 μm wide. Ilmenite mineral liberation data from the grain mounts of the 45-90 μm size fractions of the crushed basalts allows comparison of the predicted liberation and actual liberation (Table 2). The degree of liberation is defined as the fraction of ilmenite that is 80-100% clean (*i.e.*, only 0-20% attached gangue minerals).

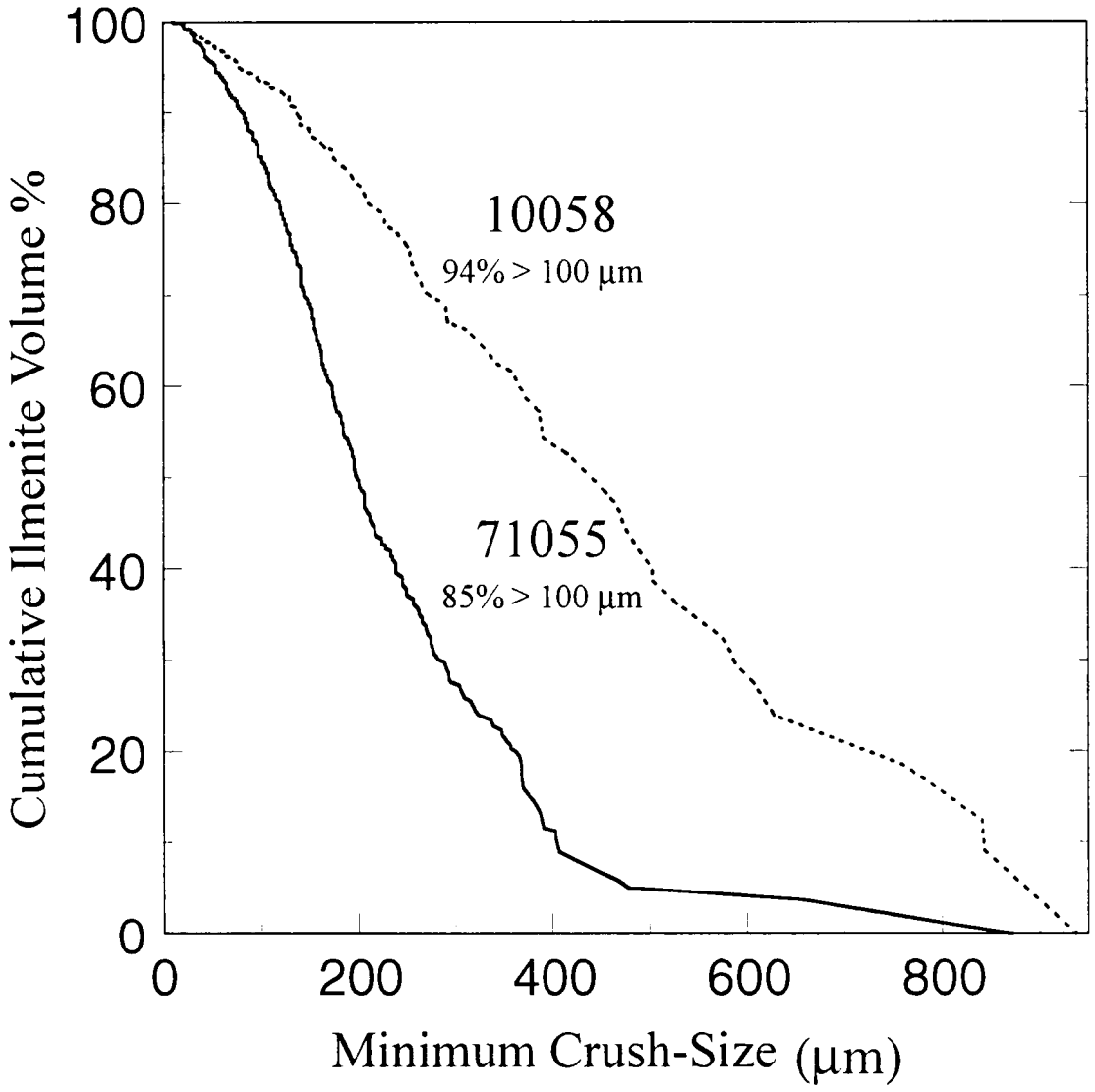



**Figure 3**. Minimum crush-size curves for ilmenite in mare basalts 71055 (fine-grain) and 10058 (medium-coarse grain). These data were calculated from size measurments made from digitized BSE images like figure 1.

The data in Table 2 indicate the 50 and 78 % of the ilmenite in comminuted (45-90 μm) 71055 and 10058 occurs as nearly free grains. Nevertheless, the actual liberation is significantly lower that that predicted from Figure 3. Ilmenite liberation is nearly 30% greater for basalt 10058 than basalt 71055, and the actual and predicted values are closer for the basalt with bladed ilmenite (94% vs. 78%-10058 and 85% vs. 50%-71055). It is apparent that crystal morphology, as well as crystal size, greatly affects mineral liberation, and therefore basalts with complex ilmenite shapes (*e.g.*, 71055) should be avoided for ilmenite extraction. Figures 4A and 4B are digitized (BSE) images from polished grain mounts of the 45-90 μm splits of 71055 and 10058. These images are generally representative of the whole grain mounts, and they display the mineral liberation and association of crushed and sized basalts 71055 and 10058. Specifically, ilmenite in 71055 is contained in multimineralic grains (mainly with pyroxene and plagioclase), but ilmenite in 10058 occurs generally as monomineralic (*i.e.*, free or liberated ilmenite) particles.

## Mineral Liberation During Soil Development

Lunar soil is formed much differently than from terrestrial soil. Lunar regolith is mainly a product of bedrock comminution by meteorite and micrometeorite bombardment. However, it is not simply crushed rock (compare figure 2 and figure 4). In fact, two main space weathering processes provide the complexity of lunar soil: comminution- crushing and breaking of rocks by meteorite bombardment; agglutination- welding of rock and mineral fragments by impact-produced glass. These

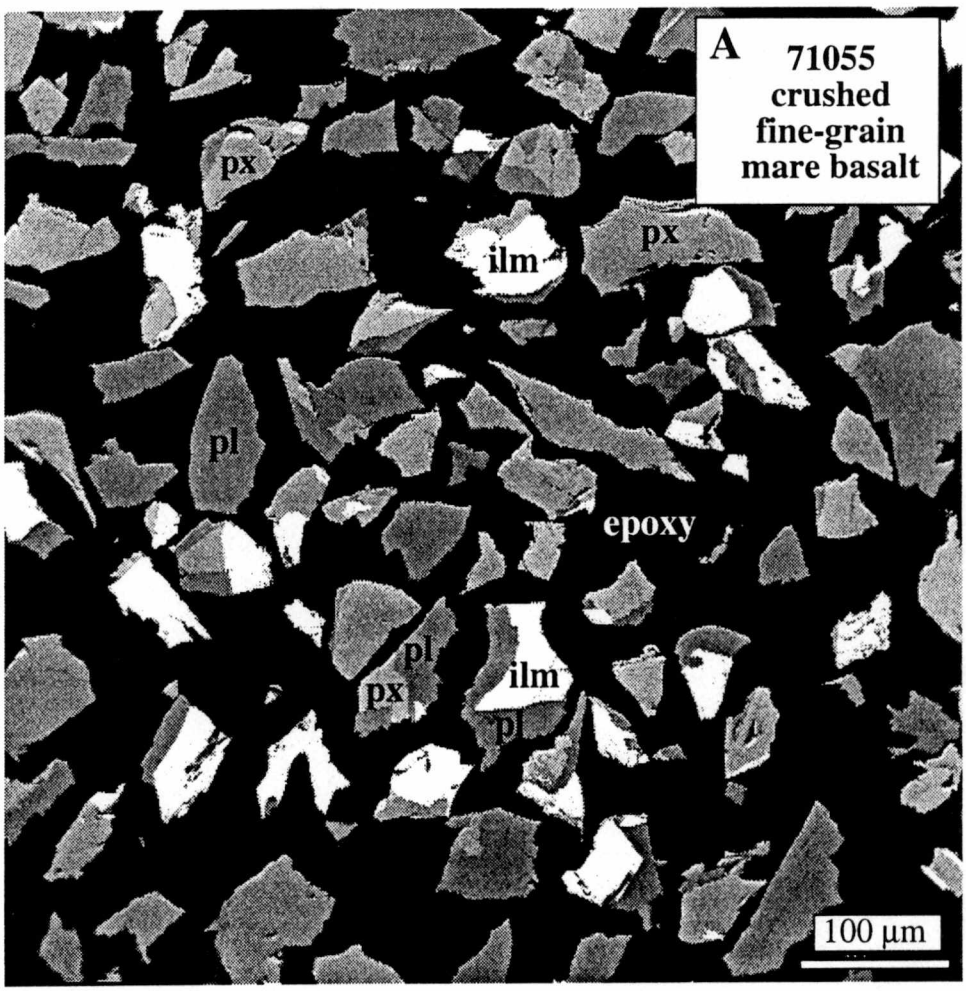



**Figure 4**. Representative digitized BSE images from grain mounts of the 45-90 µm size fractions of crushed mare basalts (**A**) 71055 and (**B**) 10058. Key: **ilm** = ilmenite (white), **px** = pyroxene (light gray), and **pl** = plagioclase (medium gray).

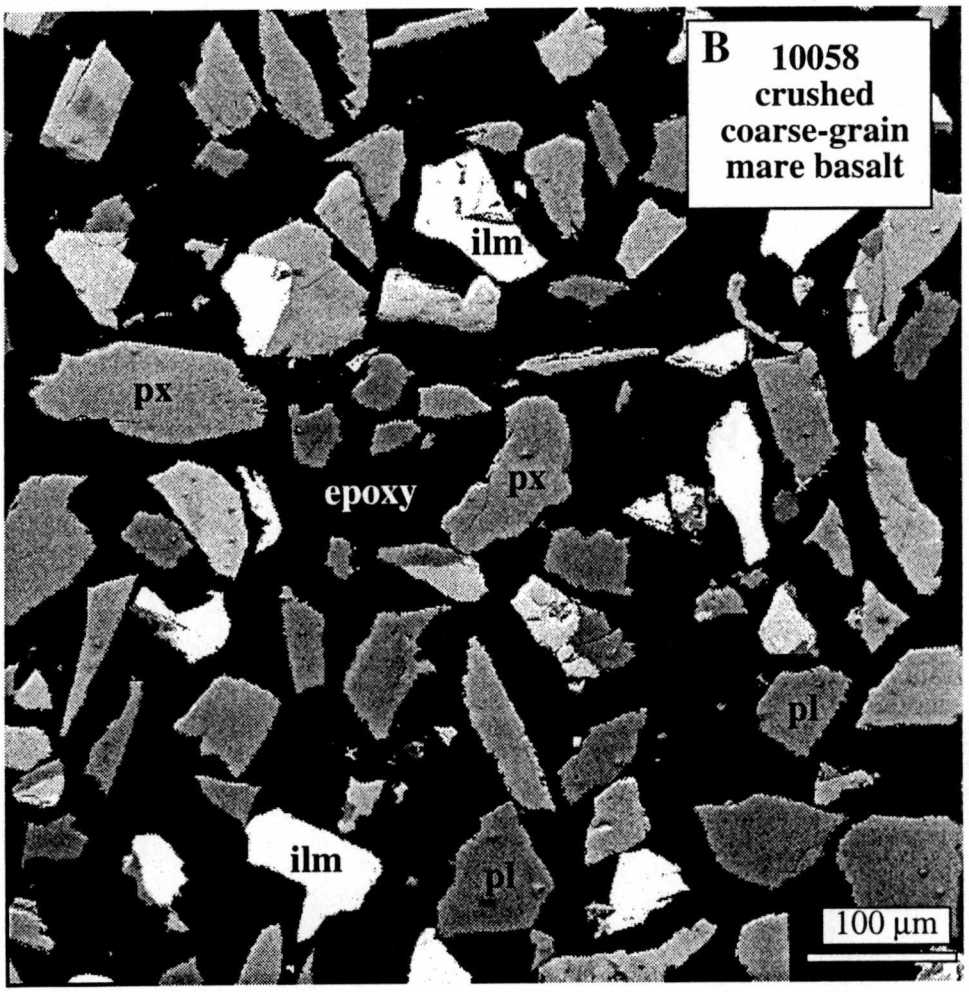

B 10058
crushed
coarse-grain
mare basalt
ilm
px
epoxy
px
pl
ilm
pl
100 µm

**Figure 4 (B).**

are competing processes since comminution releases mineral fragments from basalt, while agglutination aggregrates fragments into agglutinates and breccia.

Comminution and agglutination produce a complex mineral liberation cycle for lunar soil. During early mare-soil development, the amount of basalt fragments decrease, liberating locked minerals. Liberation does not go to completion withmaturation because agglutination welds mineral clasts together with impact-produced glass. Therefore, immature and submature soils have more free mineral particles than mature soils [*Taylor and McKay*, 1992]. Figure 5 [modified from *Taylor and McKay*, 1992] schematically illustrates how the abundance of the major petrographic components of lunar soils changes with maturity, as reflected by the $I_s$/FeO parameter. This graph shows that rock fragments and agglutinates decrease and increase sympathetically; free mineral fragment abundance goes through a maximum during immaturity-submaturity but declines with continued surface exposure due to the incorporation of mineral particles into agglutinates. This concept can be appreciated quantitatively by comparing the degree of ilmenite liberation of immature 71061, submature 71501, and mature 10084, provided in Table 2. In fact, the immature and submature soils have over 20% better ilmenite liberation than the mature soil, 10084. It is clear from the images in Figure 2 that ilmenite in 10084 is generally locked in agglutinates and soil breccia, while ilmenite in 71061 and 71501 is well liberated. Increasing agglutination and overall complexity of lunar soils during maturation are apparent from these images.

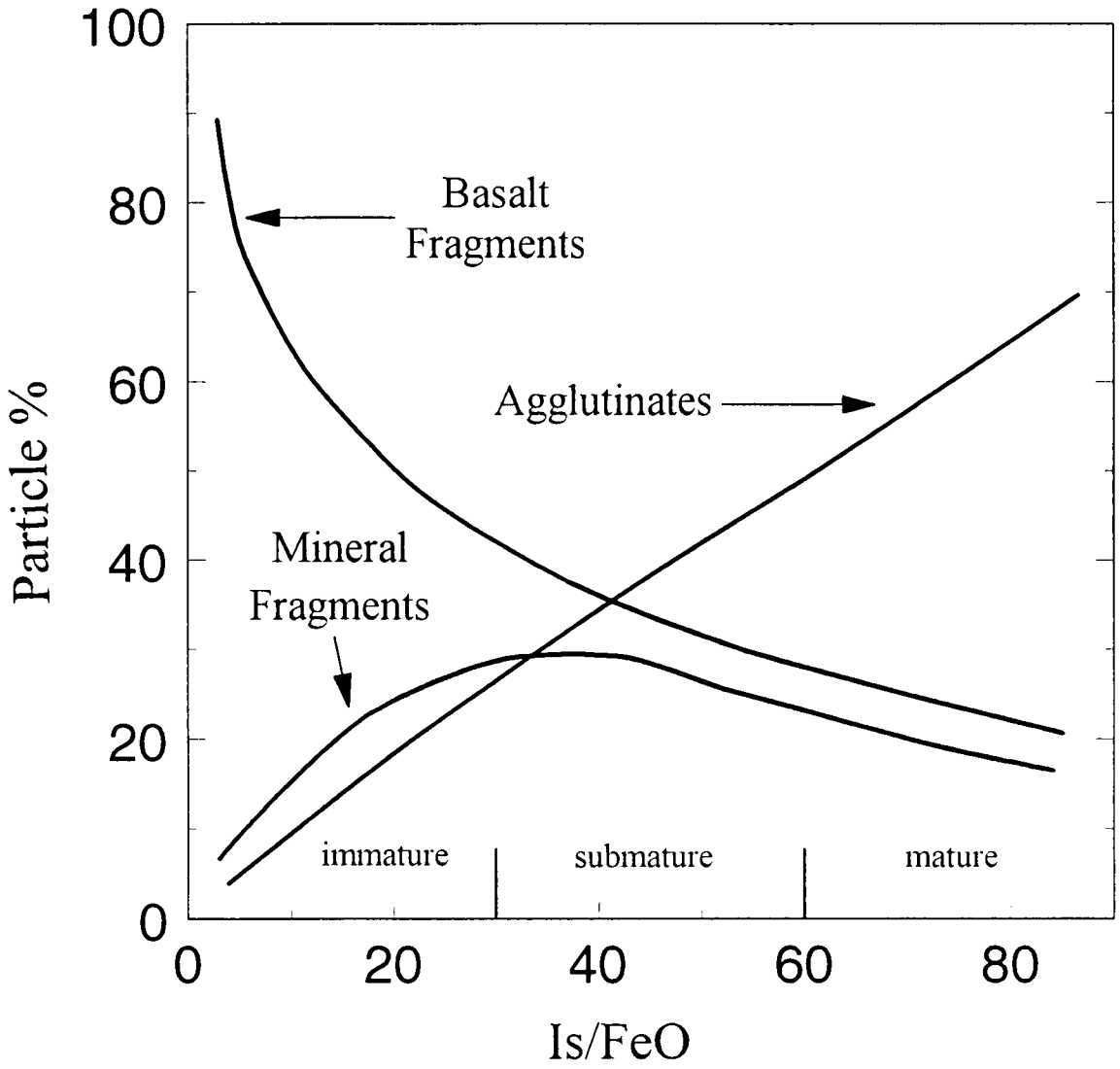



**Figure 5**. Schematic representation of the mineral liberation history of mare soils as a function of Is/FeO (*i.e.*, surface exposure) [Modified from *Taylor and McKay*, 1992]. With increasing maturity, comminution destroys basalt fragments, thereby generating free mineral particles. However, agglutination increases nearly linearly with surface exposure, incorporating free mineral fragments and basalts fragments into a glass phase. Boundaries between immature, submature, and mature soils are placed at Is/FeO values of 30 and 60 [*Morris*, 1976].

It is interesting and valuable to compare the degree of mineral liberation achieved by manual comminution and meteorite bombardment (*i.e.*, crushed basalt vs. lunar soil). Figure 6 displays ilmenite liberation curves for the 45-90 and 45-74 μm splits of the mare basalts and soils. The degree of liberation is marked as a filled circle (and listed in Table 2). The data indicate that immature and submature mare soils have ilmenite liberation similar to that of crushed basalts, specifically between 71055 and 10058. The mature soil, 10084, has considerably lower ilmenite liberation than either basalt (10-40% lower).

## Magnetic Separation of Lunar Minerals

The harsh lunar environment precludes, at least initially, mineral separation processes which are complicated and energy intensive. Magnetic separation may be a feasible mineral beneficiation technique for lunar endeavors, due to simplicity and low power requirements [*De La'O et al.*, 1990]. *Oder and Taylor* [1990] determined magnet requirements for lunar mineral separation. Most importantly, *Taylor and Oder* [1990], *Taylor et al.* [1992], and *Chambers et al.* [1994] demonstrated the ability to effectively concentrate various lunar minerals with a calibrated Frantz Isodynamic Separator. Application of X-ray digital-imaging to polished grain mounts from their magnetic splits provides quantitative comparison of possible ilmenite-rich feedstocks from basalts and soils.

The grade (ilmenite weight %), enrichment ratio (ilmenite weight % concentrate/ilmenite weight % raw material), mass yield (as weight % of

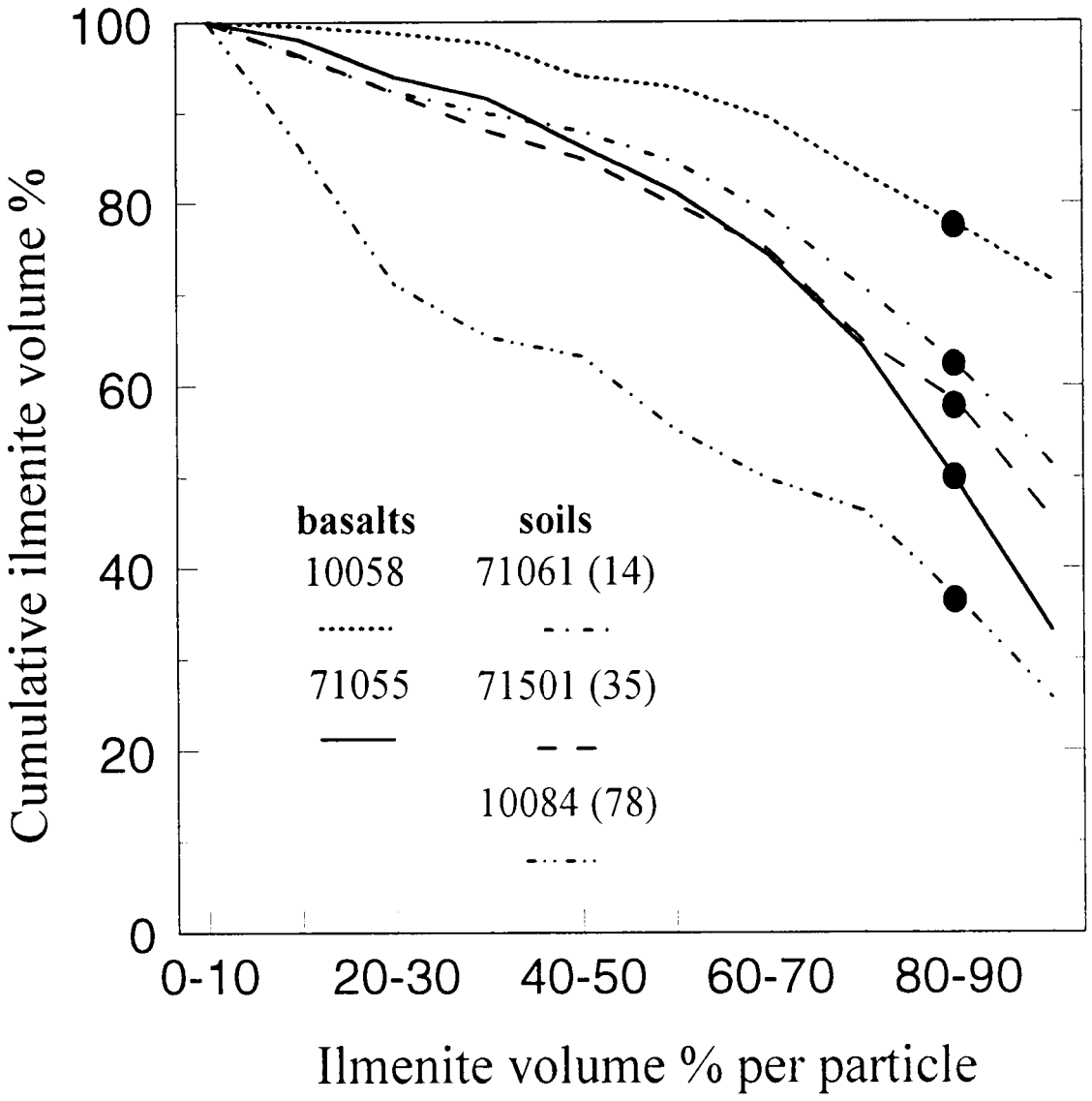



**Figure 6**. Ilmenite liberation curves for crushed mare basalts (45-90 μm) and mare soils (45-74 μm). The degree of liberation (80-100 % free) is marked as a filled circle on each curve. Is/FeO values for each soil are in parentheses.

initial rock or soil mass), and magnetic susceptibility ranges (μcc/g) of ilmenite-rich feedstocks obtained from high-Ti basalts and soils are presented in Table 3. Ilmenite concentration in basalt-derived feedstock is greater than 60 weight %, but none of the soil-derived feedstocks are richer than 35 weight % ilmenite. This is not an artifact of initial ilmenite abundance, as the basalts and immature-submature soils have similar ilmenite concentrations (Table 2). The enrichment ratio (E.R.) normalizes the concentrate grade to starting ilmenite weight %; therefore, it is a measure of mineral separation proficiency. The E.R.s for the basalts are $\geq$ 3.3, but the soils have E.R.s $\leq$ 2.3. It is apparent that ilmenite is concentrated more effectively from lunar basalt than from soil. It is difficult to compare feedstock yield of the rocks and soils due to slightly different sizing. However, it is clear that feedstock from basalt 10058 has a much greater mass yield than any other sample, a function of good ilmenite liberation upon crushing. Feedstock mass yield of soil increases with $I_s$/FeO, mainly due to the fact that the weight percentage of the 45-74 μm fraction of lunar soil increases with maturity (*i.e.*, mean grain size generally decreases with surface exposure [*McKay et al.*, 1974]).

The magnetic susceptibility of a particle is a function of mineral content, crystallinity, chemistry, shape, and size. Of these variables, mineral content is very important for lunar magnetic beneficiation studies. *Taylor et al.* [1992] showed that clean plagioclase, pyroxene, and ilmenite from lunar basalts have distinctly different magnetic susceptibilities. Nevertheless, minor attached or included high-magnetic susceptibility phases (*e.g.*, Fe-metal) dominate the magnetic signature of otherwise clean mineral fragments. For example, during magnetic experiments with mare basalts,

*Taylor et al.*, [1992] noted up to 11% cristobalite ($SiO_2$) in the most magnetic split of ground and sized rock 10058. This apparently anomalous situation resulted from micrometer-scale Fe-metal inclusions in the cristobalite. Troilite (1-5 μm wide) ± Fe-metal inclusions attached to ilmenite and clinopyroxene adversely affect their separation in crushed basalt 70155 [*Chambers et al.*, 1994a]. In addition to minor phase association, poor liberation of ilmenite from silicates inhibits production of ilmenite feedstock with high grade or mass yield (*e.g.*, compare mass yield of ilmenite concentrates from 71055 and 10058 - Table 3).

**Table 3.** Ore grade, enrichment ratio (E.R.), and mass yield of magnetically generated ilmenite-rich feedstocks from the 45-74 and 45-90 μm fractions of the mare soils and basalts.

| sample | ore grade[†] | E.R.[‡] | mass yield[§] | χ* |
|---|---|---|---|---|
| **basalt** | | | | |
| 71055 (fine-grain) | 76.5 | 3.3 | 5.5 | 50-93 |
| 10058 (med-grain) | 62.2 | 3.4 | 11.6 | 50-93 |
| **soil** | | | | |
| 71061 ($I_s$/FeO=14) | 32.4 | 2.0 | 1.8 | 60-122 |
| 71501 ($I_s$/FeO=35) | 23.9 | 1.7 | 3.4 | 60-161 |
| 10084 ($I_s$/FeO=78) | 23.5 | 2.3 | 3.8 | 75-163 |

[†]Ore grade = ilmenite weight %.
[‡]E.R. (enrichment ratio) = ilm weight % in feedstock / ilm weight % in bulk size fraction (head sample).
[§]Mass yield = feedstock weight % of the total rock or soil mass (*i.e.*, 5.5 kg of 71055 feedstock can be extracted from 100 kg of 71055 basalt).
*χ = magnetic susceptibility range in units of μcc/g.

Even though immature and submature soils have ilmenite liberation comparable to that of crushed lunar basalt, the ability to magnetically concentrate soil ilmenite is considerably less. This same is true for plagioclase and pyroxene (data not provided herein). This paradox apparently arises from the complex distribution of ferromagnetic native Fe in lunar soil. During impact events, a portion of the FeO in the silicate melt is reduced to Fe°, a result of the fusion of the soil components in the presence of solar-wind implanted hydrogen and carbon [*e.g.*, *Housley et al.*, 1973]. Even immature soils contain agglutinitic glass (Figure 2A), known for its myriad of single-domain (30-400Å) Fe° spheres [*Taylor*, 1988]. Furthermore, recent work demonstrates the occurrence of lunar soil grains with thin (100-2000 Å) amorphous rims containing spheres and blebs of metallic Fe° [*Keller and McKay*, 1993; *Christofferson et al.*, 1994; *Bernatowitz et al.*, 1994]. This Fe° is interpreted to be the result of vapor deposition or *in situ* reduction. Apparently, Fe°-bearing agglutinitic glass and amorphous rims adhering to nearly clean soil mineral fragments complicate magnetic separation, preventing high-grade feedstock production. This problem is analogous to Fe+FeS attached to otherwise clean pyroxene and ilmenite fragments in crushed basalt.

## Oxygen Liberation Experiments

Producing LLOX by hydrogen reduction of ilmenite is the ultimate goal and motivation for generating ilmenite-rich feedstock from lunar basalt and soil. An equation representing this reaction is:

$$\mathbf{FeTiO_3 + H_2 \rightarrow H_2O + TiO_2 + Fe^\circ} \qquad \mathbf{1.)}$$

The $H_2O$ can be separated into $O_2$ and $H_2$ by electrolysis, the $O_2$ pressurized and condensed to LLOX. Hydrogen gas can be recycled for further reaction with ilmenite.

Hydrogen reduction experiments using actual lunar samples provide information about reaction rates and extent. *Gibson et al.* [1994a,b] described experiments with high-Ti mare basalt 70035. They reported that reaction 1 essentially goes to completion within 20-30 minutes using finely crushed high-Ti basalt (<500 μm, mean grain size ~ 240 μm) at a temperature range of 900-1050 °C. Similarly, *Allen et al.* [1994a,b,c] stated that hydrogen reduction of ilmenite in mare soil 75061 is generally complete within 30 minutes at a temperature range of 900-1050 °C. These workers used the < 250 μm fraction of this soil. The mean grain size of the bulk soil (all material < 1 cm) is 122 μm (*McKay et al.*, 1974). In addition to the oxygen released upon reduction of FeO to Fe°, oxygen was also liberated by reduction of $TiO_2$ to "magneli" phases with a general formula of $Ti_nO_{2n-1}$ [*Anderson and Jahnburg*, 1963]. Fine grained Fe° (~1-2 μm) occurred in reacted olivine, pyroxene, and agglunitic glass, indicating partial reduction of these phases as well.

These experiments were interpreted to indicate that oxygen yields are predictable in terms of $TiO_2$ abundance (∝ ilmenite %). The reduction of all FeO in ilmenite (for ideal stoichiometry) released 10.5 weight % oxygen. Assuming that $TiO_2$ in ilmenite is reduced to $Ti_4O_7$, an additional 2.6% oxygen is acquired. Therefore, considering only the reduction of ilmenite to Fe° and $Ti_4O_7$, the oxygen yield of mare material is given by:

**O yield (weight %) = 0.131 x ilmenite weight %** **2.)**

Experimental results indicate that at least this much oxygen is generally liberated [*Gibson et al.*, 1994a,b; *Allen et al.*, 1994a,b,c]. Oxygen yields higher than predictions are common, and this is probably due to further reduction of $Ti_4O_7$ to more reduced $Ti_nO_{2n-1}$ phases (e.g., $Ti_3O_5$) and partial reduction of olivine, pyroxene, and glass. Table 4 presents predicted oxygen yields (calculated with Equation 2 and data in Tables 2 and 3) of various ilmenite-rich feedstocks and raw lunar mare basalts and soils. In addition, the experimentally determined oxygen yield of Apollo-17 orange glass, 74220(mean grain size = 40 μm, reaction temp. = 1100 °C), is provided in Table 4 [*Allen et al.*, 1994a,b,c].

Several important implications are taken from the data in Table 4. First, basalt-derived feedstock provides the most oxygen. Magnetic beneficiation of mare soils basically doubles the oxygen yield, as compared with raw soil. Interestingly, reduction of bulk Apollo-17 orange soil at 1100 °C will provide more oxygen than beneficiated high-Ti mare soils and greater than half that of beneficiated mare basalts. Of the raw, unbeneficiated materials considered, 74220 ( Fe-rich orange soil) will provide the most oxygen.

## Feedstock Comparison

The feedstock used for LLOX production by hydrogen reduction must be naturally abundant, easily excavated, provide high oxygen yield, and require minimal processing. Three materials have been evaluated herein: high-Ti mare soil, high-Ti mare basalt, and orange (Fe-rich) pyroclastic glass. The advantages and disadvantages

**Table 4.** Oxygen yield predictions and feedstock tonnage for hydrogen reduction of various lunar materials.

| feedstock | O yield (wt.%) | tonnage feed per ton oxygen[†] |
|---|---|---|
| **unbeneficiated basalt[‡]** | | |
| 71055 (fine-grain) | 3.1 | 32.3 |
| 10058 (med-grain) | 2.4 | 41.7 |
| **unbeneficiated soil[‡]** | | |
| 71061 ($I_s$/FeO=14) | 2.1 | 47.6 |
| 71501 ($I_s$/FeO=35) | 2.6 | 38.5 |
| 10084 ($I_s$/FeO=78) | 1.3 | 76.9 |
| 74220[§] | 5.4 | 18.5 |
| **beneficiated basalt*** | | |
| 71055 (fine-grain) | 10.0 | 10.0 |
| 10058 (med-grain) | 8.1 | 12.3 |
| **beneficiated soil*** | | |
| 71061 ($I_s$/FeO=14) | 4.2 | 23.8 |
| 71501 ($I_s$/FeO=35) | 3.1 | 32.3 |
| 10084 ($I_s$/FeO=78) | 3.1 | 32.3 |

[†]Number of tons of feedstock that must be reduced to generate a ton of oxygen.
[‡]Sized (45-90 μm for basalt and 45-74 μm for soil) but not magnetically treated.
[§]Oxygen yield experimentally determined by *Allen et al.* [1994a,b,c] on unsized orange soil.
*Sized and magnetically concentrated ilmenite-enriched feedstock.

of these possible feedstocks are discussed in detail below.

The ilmenite concentration (~10-20 weight %) of high-Ti mare rocks and soils makes these materials ideal for hydrogen reduction to produce LLOX. The maria cover 17 % of the lunar surface, and high-Ti basalts and soils comprise 20% of the visible mare deposits [*BVSP*, 1981]. Furthermore, even low-Ti lunar basalts are rich in $TiO_2$ (and therefore ilmenite) by terrestrial standards (*e.g.*, mean $TiO_2$ in Apollo 12 basalts is 3.5 weight % [*Lofgren and Lofgren*, 1981]). The mare regolith is 3-5 meters deep, and the basalt flows are estimated to be from hundreds of meters to several kilometers thick [*Taylor*, 1982]. Therefore, both high-Ti basalt and soil abundances are adequate for large-scale mining.

Ilmenite concentration and liberation of comminuted basalts and immature-submature soils are comparable (Table 2); but soil ilmenite is apparently not magnetically separated as effectively as basalt ilmenite (Table 3). If ilmenite-rich feedstock (~ 50 weight % ilmenite) is required, then magnetically beneficiated high-Ti basalt is probably required. Raw high-Ti mare soil is an excellent material since it will provide oxygen yield similar to crude basalt, but without requiring energy-intensive excavation and manual comminution.

Orange pyroclastic glass is receiving much attention as a lunar resource because of its high oxygen yield (5.4%), unconsolidated nature, and volatile coatings [*Allen et al.*, 1994a,b,c; *Cooper*, 1994]. Pyroclastic deposits are not as extensive as mare basalts and soils, but *Hawke and Coombs* [1994] note formations with areas up to 30,000 $km^2$. Furthermore, pyroclastic glasses may be tens of meters deep, much thicker than mare

regolith. The obvious advantage of orange glass feedstock is the low processing cost due to its uniformly fine-grained, unconsolidated nature (*i.e.*, no crushing, sizing, or screening required).

Hydrogen reduction experiments by *Allen et al.* [1994a,b,c] reveal some potential problems of using Fe-rich glasses for LLOX production; namely, reaction temperature and time are greater than for high-Ti mare soil and basalt, and oxygen yield is strongly dependent on temperature. Another caveat is the phenomenon of glass sintering during reactions conducted at temperatures from 1050-1100 °C (the temperature range required for ~ 5% oxygen yield from 74220). Sintering of 74220 (orange soil) required the reduced glass to be chipped from the reaction vessels [*Allen et al.*, 1994c]. Longer reaction time, higher reaction temperature, and sintering of feedstock may be detrimental to a lunar oxygen production plant. However, it is possible that fluidized reactor beds [*e.g.*, *Gibson and Knudsen*, 1990] could minimize these factors.

In short, if minimally processed feedstock (*i.e*, not treated magnetically) is desired, orange soil and high-Ti mare soil are the best materials. Oxygen production plants that require ilmenite-rich concentrates (~ 50 weight % ilmenite) will presumably use beneficiated, coarse-grained basalt, as soil ilmenite is not well separated upon magnetic treatment -- *i.e.*, the mass yield of a sufficiently higher grade would be prohibitively low.

# CONCLUSIONS

X-ray digital-image analyses of grain mounts of lunar soil and crushed lunar basalt provide, for the first time, quantitative comparison of actual ilmenite abundances and liberation of these materials. Immature-submature high-Ti mare soils have ilmenite abundance and liberation comparable to crushed high-Ti basalts, but the ability to magnetically concentrate soil ilmenite is limited. Lack of good separation of clean mineral particles from lunar soil is due to the complexity of soil formation as compared to simple basalt comminution. Specifically, Fe°-bearing agglutinitic glass and amorphous rinds on soil grains complicate magnetic beneficiation.

Oxygen yield predictions for various feedstocks show that the basalt-derived ilmenite-rich concentrates should provide the most oxygen. It is especially noteworthy that raw orange soil yields more oxygen than beneficiated mare soils and over half as much as the beneficiated mare basalts. Oxygen yield predictions of unbeneficiated immature-submature high-Ti mare soils and basalts are similar. Upon consideration of mare soil, mare basalt, and orange soil as feedstocks for LLOX production, it is apparent that high-Ti mare and orange soils should be most feasible during early lunar occupation due to minimal processing costs. These materials will not require crushing, which is energy-intensive and demands massive equipment. Basalt excavation and ilmenite-rich feedstock generation may only be practical after a permanent base is established, the nature of basalt flows is explored, and true mining costs can be evaluated.

# REFERENCES


Allen, C.C., G.G. Bond, and D.S. McKay, Lunar oxygen production-A maturing technology, in *Engineering, Construction and Operations in Space IV*, pp. 1157- 1166, American Society of Civil Engineers, New York, 1994a.

Allen, C.C., R.V. Morris, and D.S. McKay, Reduction of lunar mare soil and pyroclastic glass (abstract), *Lunar Planet. Sci. Conf. XXV*, pp. 23-24,1994b.

Allen, C.C., R.V. Morris, and D.S. McKay, Experimental reduction of lunar mare soil and volcanic glass, Submitted to *J. Geophys. Res.*, 1994c.

Anderson, S. and Jahnburg, L., Crystal structure studies on the homologous series $Ti_nO_{2n-1}$,$V_nO_{2n-1}$, and $Ti_{n-2}Cr_2O_{2n-1}$, *Ark. Kemi., 21*, pp. 413-426, 1963.

Bates, R.L. and J.A. Jackson (eds.), *Glossary of Geology* 3rd Edition, American Geological Institute, Alexandia, VA, 1987.

Bernatowicz, T.J., R.H. Nichols Jr., and C.M. Hohenburg, Origin of amorphous rims on lunar soil grains (abstract), *Lunar Planet. Sci. Conf XXV*, pp. 105-106, 1994.

BVSP (Basaltic Volcanism Study Project), *Basaltic Volcanism on the Terrestrial Planets*, Pergamon, New York, pp. 1286, 1981.

Chambers, J.G., L.A. Taylor, A. Patchen, and D.S. McKay, Mineral liberation and beneficiation of lunar high-Ti mare basalt, 71055: Digital-imaging analyses, in *Engineering, Construction, and Operations in Space IV*, pp. 878-888, American Society of Civil Engineers, New York, 1994a.

Chambers, J.G., A. Patchen, L.A. Taylor, S.J. Higgins, and D.S. McKay, Lunar mineral feedstocks from rocks and soil: X-ray digital-imaging in resource evaluation (abstract), *Lunar Planet. Sci. Conf. XXV*, pp. 235-236, 1994b.

Christofferson, R.S., D.S. McKay, and L.P. Keller, Grain rims on ilmenite in the lunar regolith: Comparison to vapor deposits on regolith silicates (abstract), *Lunar Planet. Sci. Conf. XXV*, 1994.

Cooper, B., Reservoir estimates for the Sulpicious Gallus region, in *Engineering, Construction, and Operations in Space IV*, pp. 889-896, American Society of Civil Engineers, New York, 1994.

De La'O, K.A., T.C. Eisele, D.B. Kasul, W.I. Rose, and S.K. Kawatra, Separation of lunar of lunar ilmenite: Basalt vs. regolith, in *Engineering, Construction, and Operations in Space II*, pp. 177-186, American Society of Civil Engineers, New York, 1990.

Duke, M.B, C.C. Won, G. A. Sellers, M.L. Bird, and R.B Finkelmean, Genesis of lunar soil at Tranquility Base, *Proc. of Apollo 11 Lunar Sci. Conf.*, p. 347-361, 1097.

Frondel, C., C. Klein Jr., J. Ito, and J.C. Drake, Mineralogical and chemical studies of Apollo 11 lunar fines and selected rocks, *Proc. Apollo 11 Lunar Sci. Conf. 1st*, pp. 445-474, 1970.

Gibson, M.A. and C.W. Knudsen, Automation and control potential for the Carbotek lunar oxygen production process, in *Engineering, Construction, and Operations in Space II*, pp. 197-205, American Society of Civil Engineers, New York, 1990.

Gibson, M.A., C.W. Knudsen, D.J. Brueneman, and H. Kanamori, Kinetic interpretations of first reactivity and experiments on lunar basalt samples, in *Engineering, Construction, and Operations in Space IV,* pp. 1167-1177, American Society of Civil Engineers, New York, 1994a.

Gibson, M.A., C.W. Knudsen, D.J. Brueneman, C.C. Allen, H. Kanamori, and D.S. McKay, Reduction of lunar basalt 70035: Oxygen yield and reaction product analysis, *J. Geophys. Res.*, 99, E5, 10,887-10,897, 1994b.

Hawke, B.R. and C.R. Coombs, A remote sensing evaluation of lunar pyroclastic deposits, in *Engineering, Construction, and Operations in Space IV*, pp. 1108-1019, American Society of Civil Engineers, New York, 1994.

Heiken, G.H. and D.S. McKay, Petrography of Apollo 17 soils, *Proc. Lunar Planet. Sci. Conf. 5th*, pp. 843-860, 1974.

Heiken, G.H. and D.T. Vaniman, Characterization of lunar ilmenite resources, *Proc. Lunar Planet. Sci. Conf. 20th*, pp. 239-247, 1990.

Heiken, G.H., D.T. Vaniman, and H. Hawkins, Sulfur as a lunar resource, in *Engineering, Construction, and Operations in Space III*, pp. 555-564, American Society of Civil Engineers, New York, 1992.

Higgins, S.J., A. Patchen, J.G. Chambers, L.A. Taylor, and D.S. McKay, Petrographic characterization of lunar soils: Application of X-ray digital-imaging to quantitative and automated analysis (abstract), *Lunar Planet. Sci. Conf. XXV*, pp. 547-548, 1994.

Higgins, S.J., J.G. Chambers, L.A. Taylor, A. Patchen, and D.S. McKay, X-ray digital-imaging petrography Part I: Technique development for lunar (mare) soils, *in press.*

Housley, R.M., R.W. Grant, and N.E. Paton, Origin and characteristics of excess Fe metal in lunar glass welded aggregates, *Proc. Lunar Planet. Sci. Conf. IV*, pp. 2737-2749, 1973.

Hu, H.N. and L.A. Taylor, Lack of chemical fractionation in major and minor elements during agglutinate formation, *Proc. Lunar Planet. Sci. Conf. VIII*, pp. 3645-3656, 1977.

Johnson, G.R. and G.R. Olhoeft (R.S. Carmichael, ed.), Density of rocks and minerals (Ch. 1), *Handbook of Physical Properties of Rocks*, CRC Press, Boca Raton, 1982.

Keller, L.P. and D.S. McKay, Discovery of vapor deposits in the lunar regolith, *Science*, 261, pp. 1305-1307, 1993.

Lofgren, G.R. and E.M. Lofgren, *Catalog of lunar mare basalts greater than 40 grams-Part 1: Major and Trace Chemistry*, Lunar and Planetary Contribution 438, pp. 418, 1981.

McKay, D.S., R.M. Fruland, and G.H. Heiken, Grain size and the evolution of lunar soils, *Proc. Lunar and Planet. Sci. Conf.* V, pp. 887-906, 1974.

Morris, R.V., Surface exposure indices of lunar soils: A comparative FMR study, *Proc. Lunar and Planet. Sci. Conf.* V11, pp. 315-335, 1976.

Morris, R.V., The surface exposure (maturity) of lunar soils: Some concepts and $I_s$/FeO compilation, *Proc. Lunar Planet. Conf. IX*, p. 2287- 2297, 1978.

Neal, C.R. and L.A. Taylor, *Catalog of Apollo 17 rocks, Volume 2-Central Valley, Part 1*, JSC-NASA Reference Publication # 26088, 1993.

Oder, R.R. and L.A. Taylor, Magnetic beneficiation of highland and high-Ti soils: Magnet Requirements, in *Engineering, Construction, and Operations in Space II*, pp. 133-142, American Society of Civil Engineers, New York, 1990.

Petruk, W., Automatic image analysis for mineral beneficiation, *Review of Extractive Metallurgy*, 40, pp. 29-31, 1988a.

Petruk, W., The capabilities of the microprobe Kontron image analysis system: Application to mineral beneficiation, *Scanning Microscopy*, 2, pp. 1247-1256, 1988b.

Simon, S.B., J.J. Papike, and J.C. Laul, The lunar regolith: Comparative studies of the Apollo and Lunar sites. Petrology of soils from Apollo 17, Lunar 16, 20, and 24, *Proc. Lunar Planet. Sci. Conf. XII*, p. 371-388, 1981.

Sutherland, D.N. and P. Gottlieb, Application of automated quantitative mineralogy in mineral processing, *Minerals Engineering*, 4, pp. 753-762, 1991.

Taylor, L.A., Generation of native Fe in lunar soil, in *Engineering, Construction, and Operations in Space I*, pp. 67-77, American Society of Civil Engineers, New York, 1988.

Taylor, L.A. and Oder, R.R., Magnetic beneficiation of highland and high-Ti mare soils: Rock, mineral, and glassy components, in *Engineering, Construction, and Operations in Space II*, pp. 143-152, American Society of Civil Engineers, New York, 1990.

Taylor, L.A. and D.S. McKay, An ilmenite feedstock on the Moon: Beneficiation of rocks versus soils (abstract), *Lunar Planet. Sci. Conf. XXIII*, pp. 1411-1412, 1992.

Taylor, L.A., D.S. McKay, J. Graf, A. Patchen, S. Wentworth, R.R. Oder, and E.A. Jerde, Magnetic beneficiation of high-Ti mare basalts: Petrographic analysis (abstract), *Lunar Planet. Sci. Conf., XXIII*, pp. 1415-1416, 1992.

Taylor, L.A. and W.D. Carrier III, The feasibility of processes for production of oxygen on the Moon, in *Engineering, Construction, and Operations in Space III*, pp. 752-762, American Society of Civil Engineers, New York, 1992.

Taylor, L.A., J.G. Chambers, A. Patchen, E.A. Jerde, D.S. McKay, J Graf, and R.R. Oder, Evaluation of lunar rocks and soils for resource utilization: Detailed image analysis of raw material and beneficiated products, *Lunar Planet. Sci. Conf. XXIV*, pp. 1409-1410, 1993.

Taylor, R.S., *Planetary Science: A Lunar Perspective*, Lunar and Planetary Institute, Houston, p.481, 1982.

Vaniman, D.T. and G.H. Heiken, Getting lunar ilmenite from soils or rocks?, in *Engineering, Construction, and Operations in Space II*, pp. 107-116, American Society of Civil Engineers, New York, 1990.

Walker, R.J. and J.J. Papike, The relationship of the lunar regolith < 10 μm fraction and agglutinates. Part II: Chemical composition of agglutinate glass as a test of the "fusion of the finest fraction" $F^3$ model, *Proc. Lunar Planet. Sci. XII*, pp. 421-432, 1981.

Wills, B.A., *Mineral Processing Technology, 5th Edition*, Oxford, Pergamon Press, p.855, 1992.

# PART 4

# X-RAY DIGITAL-IMAGING OF LUNAR MARE SOILS: TRUE MODAL ANALYSES OF APOLLO 11, 12, 15, AND 17 SAMPLES

# ABSTRACT

Previous petrographic studies of the lunar soil, the < 1 cm fraction of the regolith, have employed particle-counting as the standard procedure for characterization. These data have been generally referred to as the soil modal compositions. However, this technique does not produce true modal data, as the percentage of a mineral locked in lithic fragments and fused-soil-particles is not determined. Detailed modal analyses have been performed by X-ray digital-imaging on a suite of nine mare soils from the Apollo 11, 12, 15, and 17 sites. This is the first collection of such data from all mare sites. Comparison of these new data with particle-count data indicate that the latter are inadequate for estimating actual mineral abundances. In fact, the total mineral content is underestimated by factors of 2-17 if it is assumed that the particle counts are equivalent to modal analyses. This observation is critical, as accurate modal data are required for resource evaluation and for calibration of remote sensing methods. Evaluation of the modal data and particle-count data (also determined by digital-imaging methods during this study) of the mare soil suite indicates that the Al-rich glass content, agglutinate content, and the normative/modal ratio increase with $I_s$/FeO, the ferromagnetic maturity index. These correlations are the direct result of the impact melting and auto-reduction of FeO, associated with surface exposure and subsequent meteorite and micrometeorite collisions. The Apollo 12 soils consistently appear petrographically more mature than is indicated by their $I_s$/FeO values. This phenomenon is interpreted to be the result of a slightly greater 100 meter-

scale crater density, providing for melting of fresh soil and rock fragments, (*i.e.*, material lacking reducing solar-wind hydrogen and carbon) at the Apollo 12 site. This is an important example of the local cratering history overprinting the otherwise rather quiescent formation of lunar soil.

## INTRODUCTION

The lunar surface is blanketed by a mixture of loosely consolidated rock, mineral. and glass fragments, termed the regolith. The lunar regolith thickness varies from 10-20 meters in the highland regions to 3-5 meters in the maria. The regolith, with its < 1 cm size fraction, the soil, is a product of meteorite and micrometeorite impacts. Since the Moon lacks water and a significant atmosphere ($10^{-12}$ to $10^{-14}$ torr), this bombardment is the only form of weathering present. In fact, the formation of lunar regolith has become the standard model for regoliths on other airless bodies. As such, study of the lunar regolith provides a better understanding of space weathering of geologic material on the Moon, asteroids, Mars, and other comparable solar system members.

In the past, it has been standard operating procedure to characterize a lunar soil by particle-counting [*e.g.*, *Heiken and McKay*, 1974]. Such analyses provide detailed information about the abundance of lithic fragments, mineral fragments, impact-produced glasses, pyroclastic glasses, and glass-bonded aggregates (*e.g.*, agglutinates). Unfortunately, results from these particle counts were generally referred to as the soil modal compositions [*e.g.*, *Heiken et al.* eds. 1991]. However, modes or modal

percentages are strictly defined as the actual abundance of mineral constituents expressed as volume or weight percentages [*Bates and Jackson*, 1990]. Particle counts *do not* provide such information, as the technique does not determine the percentage of a mineral locked in lithic fragments and fused-soil particles (*e.g.*, agglutinates). These locked mineral grains add significantly to the total concentration as reported by *Chambers et al.* [1994a, 1995a,b].

True modal analyses must be performed on lunar soils to appreciate quantitatively the mineralogical developments during maturation. This is of paramount importance for remote sensing spectral reflectivity studies of airless bodies. In addition, resource evaluation requires such data for comparison of mare soils and basalts as raw materials for mineral beneficiation. X-ray and BSE digital-imaging analysis was shown to be an adequate method for obtaining detailed mineralogical data from lunar material by *Heiken and Vaniman* [1990], *Heiken et al.* [1992], *Taylor et al.* [1993], and *Chambers et al.* [1994a,b; 1995a,b]. In addition, particle counting data are determined by this method [*Higgins et al.*, 1994, 1995].

The 90-150 μm fraction of nine mare soils from the Apollo 11, 12, 15, and 17 missions were analyzed by X-ray digital-imaging techniques in order to obtain true modal and particle-count data. This work is the first and only collection of actual modal data for soils from all Apollo mare sites. These data are used to explore the mineralogical and petrographical developments of maturing mare soils. The results show unequivocally that particle-count data do not estimate true mineral abundances. Therefore, true modal analyses of the lunar soil collection are lacking and are needed.

# ANALYTICAL METHODS

Nine polished grain mounts of the 90-150 μm fractions of mare soils from Apollo 11, 12, 15, and 17 were obtained from the Lunar Sample curator at Johnson Space Center, Houston, Texas. These soils were examined with transmitted and reflected optical microscopy to determine the mineral content and petrography of these samples, as this information is needed to perform automated X-ray mapping.

The mineral abundance data were obtained with an Oxford Instruments (LINK) Energy Dispersive Spectrometer (EDS) eXL II mounted on a Cameca SX-50 EMP in the Department of Geological Sciences, the University of Tennessee. Backscattered electron (BSE) signals were used to discriminate between epoxy and grains. Phases were identified by characteristic X-ray spectrometry with an Oxford Instruments EDS. Specifically, the Oxford software, Featurescan and Phase Distribution Analyses (formerly Mineral Liberation), uses operator-defined chemical criteria to distinguish the various phases of a sample (*e.g.*, high Ca and Al and low Fe and Mg are indicative of plagioclase). Lunar glasses such as Ti-rich glass (~7-10 % $TiO_2$) and Al-rich glass (~10-20 % $Al_2O_3$) are treated as discrete phases, although their definitions are, to a large extent, subjective. A full explanation of the chemical criteria used for A-17 soil mineral identification is given in *Higgins et al.* [1995]. It must be stressed that mineral and glass compositions vary from soil to soil, and therefore, some fine-tuning of the phase definitions is generally required.

The excitation potential, beam current, spot size, and magnification for X-ray mapping were 20 kV, 3 nA, 1 μm, and 70 X, respectively. The counting times for spectrum analysis were 40 ms for the A-11 and A-17 soils and 60 ms for A-12 and A-15 soils. Longer counting time was required to distinguish between pyroxenes and the low-Ti green/yellow glass fragments present in the A-12 and A-15 samples. For image analysis, the pixel, stepping, and image sizes were 1.9 μm, 3.8 μm, and 512 X 512, respectively. Some grain mounts did not contain enough particles to allow analysis of 1000 features, as per the criterion of *Sutherland and Gottlieb* [1991]. However, a minimum of 450 grains from each grain mount was characterized.

The various particle types of lunar soils are classified on the basis of relative mineral and glass abundances and texture. Particle classification is subjective, whether by optical or digital means. Nevertheless, digital-imaging characterization provides less intersample bias, as the particle-type determination uses the same computer code for every sample. This is performed with an off-line feature filter (provided with Featurescan) which is basically a logic-based protocol that assigns a label (*e.g.*, agglutinate or basalt fragment) to a particle according to operator-defined criteria. These criteria were developed iteratively with the use of optical microscopy, backscattered electron images, and false-colored phase maps of thousands of grains from mare lunar soils. *Higgins et al.* [1994, 1995] outlined the particle classification criteria for A-17 high-Ti mare soils. They showed that the digital-imaging and published optical petrographic data were similar. In order to generate an internally

consistent data set for this study, digital-imaging particle counts were performed on all nine mare soils.

All bulk chemical data for the mare soils and basalts used for normative calculations were obtained from various catalogs of lunar samples. Basalt modal data used to prepare Figure 3 were taken from various studies that were compiled in the Apollo 11 catalog [*Kramer*, et al. 1977], Apollo 12 catalog [*Warner*, 1970], Apollo 15 Catalog [*Ryder*, 1985], Apollo 17 Catalog-Volume 2 [*Neal and Taylor*, 1993]. Original sources are too numerous to list individually.

## LUNAR SOIL FORMATION

The lunar soil is unique as compared to terrestrial soil. The lunar soil is not a product of chemical alteration by water and weak acids and physical degradation by water and wind, but it is formed mainly by comminution of basaltic bedrock and boulders by impacting meteorites and micrometeorites. Nevertheless, mare soil is not simply crushed basalt, because hypervelocity impacts generate silicate melts, which penetrate the soil particles and quench to glass, thereby binding previously liberated mineral and rock fragments into aggregates. This process, agglutination, generates the ubiquitous fused-soil-particles appropriately termed agglutinates. Other, but less significant, weathering processes include spallation, the spalling of mineral and glass surfaces, and implantation, the deposition of various solar-derived volatile elements. Both are products of high-energy solar winds, which impinge the lunar surface virtually unattenuated.

The original minerals of lunar mare soils are inherited from the local basaltic bedrock. However, various impact-produced glasses are also present, and they are the result of the rapid quenching of melts of this basaltic mineralogy. Therefore, the overall mineral abundance is decreased with continued impacts. Soil particles experience melting from micrometeorite collisions (the most abundant impactors) only when they reside in the upper few millimeters of the regolith. Therefore, soils that have more surface exposure contain a larger portion of impact-generated glass, mainly in the form of the glass phase of agglutinates, and they are considered more mature. Impact melts are chemically variable, but the average composition (to 1 standard deviation) is approximately equivalent to the respective bulk soil chemistry [*Hu and Taylor*, 1977]. *Walker and Papike* [1981] demonstrated that a major portion of this agglutinate glass formed as a result of preferential fusion of the < 10 μm fraction of soils. This fraction of mare soils is enriched in plagioclase as a result of enhanced crushability [*e.g., Haskin and Korotev*, 1977], and therefore, soils should become more depleted in modal plagioclase (relative to other minerals) with increased maturation.

Petrographic development of lunar soils is recorded as decreased mean grain size, better sorting, decreased lithic fragments, and increased amounts of fused-soil particles (*e.g.*, agglutinates) [*McKay et al.*, 1974]. In addition, mineral resource studies demonstrated that mineral liberation increases with maturity until the process of agglutination starts canceling the net effects of comminution [*Taylor and McKay*, 1992]. Indeed, the processes of agglutination and comminution are competing in the

sense that they act to increase and decrease mean grain size, respectively. This leads to to a steady-state evolution with respect to grain size [*McKay et al*, 1974].

The bulk chemistry of lunar soil is not drastically affected by impact melting and comminution; however, the energy from large-scale impacts ballistically transports exotic soil particles of differing composition to other locations, where they are mixed with the local material. These events are rare, and they do not produce a homogeneous lunar soil, as evidenced by the rather sharp mare-highland boundaries. Nevertheless, plagioclase-rich highland material is mixed with the local basaltic mare soils, resulting in, for example, higher $Al_2O_3$, lower FeO, and lower $TiO_2$ concentration than the local basalts. These exotic mineral and rock fragments can be recognized by mineral compositions unlike those of returned rock samples from the collection area [*Labotka et al.*, 1980]. Pyroclastic glasses (*e.g.*, A-17 orange glass) are also mixed with the gray soil. These glasses are generally more mafic and less aluminous than mare basalts, and therefore, their addition tends to oppose the chemical trends of mare basalt-highland material mixing. With these concepts in mind, *Laul and Papike* [1980] performed chemical mixing calculations for specific soils to estimate the degree of multicomponent mixing in the regolith. These estimates were similar to the percentages of exotic glass and mineral fragments present in a given soil [*Papike et al.*, 1982].

Minor amounts of solar-wind elements, including H, He, C, N, Ar, Ne, Kr, and Xe, are implanted into the surfaces of mineral and glass grains present in the lunar soil. As with impact melting, only the grains in the upper few millimeters of the soil are affected by this phenomenon. The gardening of soils fragments mixes and turns the

particles exposing them to the solar wind. Therefore, the amount of these solar wind components increases with surface exposure or maturity. Nevertheless, even young high-Ti mare soils are rich in solar-wind H and He, a function of the selective retention of these elements by ilmenite [*e.g., Taylor*, 1990]. Although these elements are only present at concentrations up to ~ 100-200 ppm, they may be important for future lunar resource utilization [*e.g.*, $^{3}$He; *Taylor*, 1994].

The combined effects of solar-wind-element implantation and impact melting produces an interesting mineralogical evolution of lunar soils. During the impact fusion, a portion of the FeO in the silicate melt is reduced to Fe°, which nucleates and grows to form native Fe metal spheres 40-300 Å in diameter, a process called auto-reduction [*Housley et al.*, 1973]. This single-domain Fe is measured by ferromagnetic resonance (FMR) and quantified by intensity as $I_s$. Since both the amounts of impact glass and solar-wind elements increase with surface exposure, the percentage of Fe metal and the ferromagnetic intensity ($I_s$) of lunar soils also increases. The FeO concentration of a target soil largely controls the amount of Fe metal that can be produced by auto-reduction. By normalizing the FMR intensity ($I_s$) to the total iron concentration (as FeO) in a soil, a relative soil maturity index, $I_s$/FeO, termed the ferromagnetic maturity parameter was devised by *Housley et al.* [1975]. Values of $I_s$/FeO for collected soils range from 1 to ~ 100 arbitrary units [*Morris*, 1978]. *Morris* [1976] defined the ranges: 0-29 = immature, 30-59 = submature, and > 60 = mature. $I_s$/FeO positively correlates with agglutinate percentages and trapped solar gas content,

and it negatively correlates with mean grain size. This parameter is used throughout this study as a guide to soil maturity.

Consideration of many of the factors above allows a general petrographic-magnetic evolution of lunar soils to be postulated. This is concisely embodied by Figure 1, modified after *Taylor and McKay* [1992]. This graph shows that the competing processes of comminution and agglutination provide a rather sympathetic relationship between basaltic fragments and agglutinate abundances with increasing $I_s$/FeO (*i.e.*, surface exposure or maturity). Mineral liberation is complex. Initially the mineral constituents are locked in basalt fragments, but continued comminution liberates these grains, providing a broad peak during late immaturity-early submaturity. Eventually, agglutination melts some of these mineral fragments and aggregates others, resulting in lower clean mineral particle contents for mature soils.

## RESULTS AND DISCUSSION

As noted earlier, soils from all Apollo mare sites were included in the sample set for this study. Soil 10084 was collected at the Apollo 11 site of Mare Tranquillitatis. Soils 12001 and 12030 were collected during the Apollo 12 mission to Oceanus Procellarum. Samples 15041 and 15071 were collected in the mare adjacent to Hadley Rille, during the Apollo 15 mission. The Apollo 17 soils 70181, 71061, 71501, and 79221 were sampled in the Taurus-Littrow Valley, which is located on the southeast margin of Mare Serenitatis.

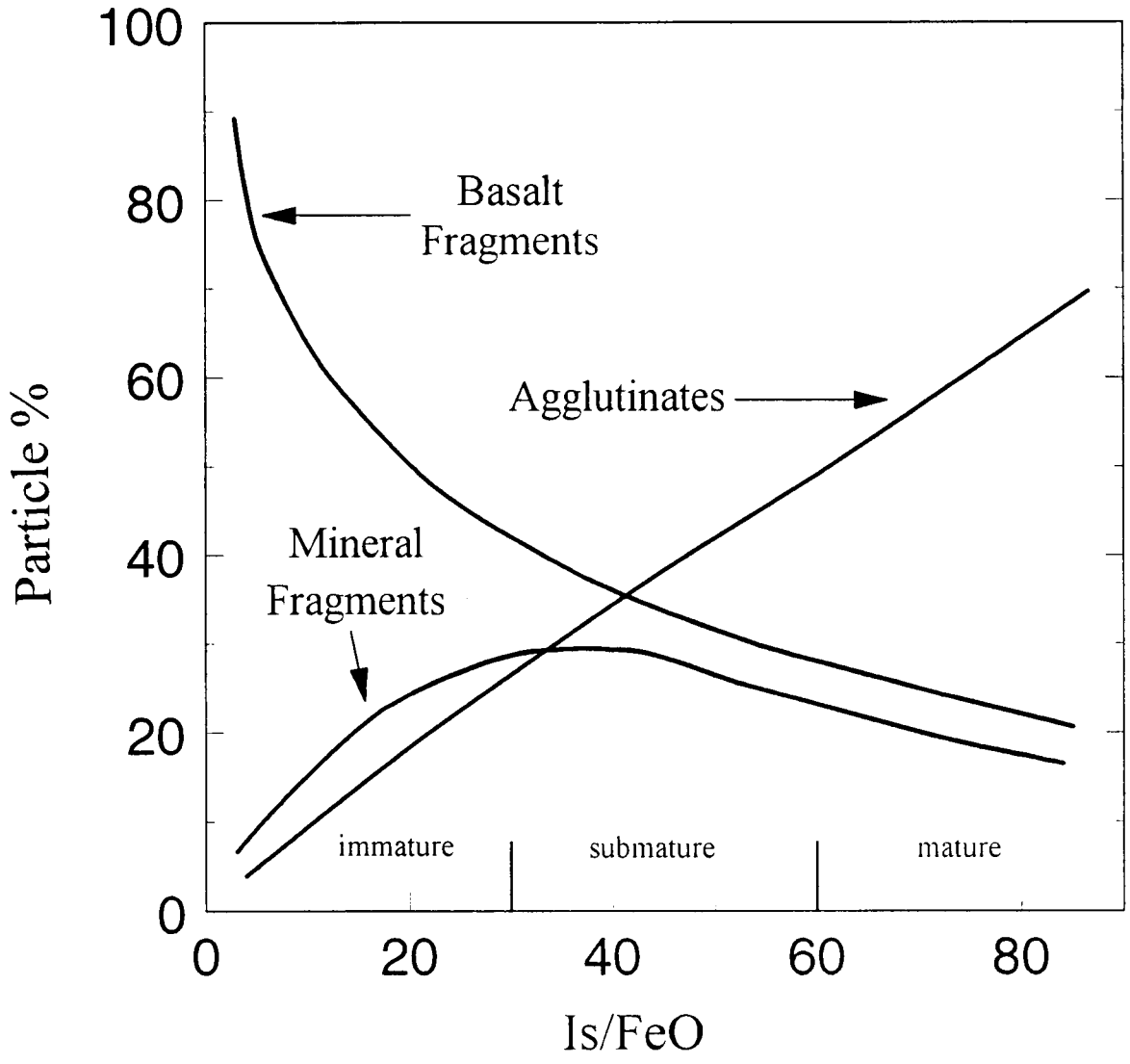



**Figure 1**. Schematic representation of the petrographic history of mare soils as a function of Is/FeO (*i.e.*, surface exposure) [Modified from *Taylor and McKay*, 1992]. With increasing maturity, comminution destroys basalt fragments, thereby generating free mineral particles. However, agglutination increases nearly linearly with surface exposure, incorporating free mineral fragments and basalts fragments into a glass phase. Boundaries between immature, submature, and mature soils are placed at Is/FeO values of 30 and 60 [*Morris*, 1976].

## Mineralogy

The mineral and glass content of lunar soil is a function of the nature of the local bedrock, exotic material additions, local and regional pyroclastic deposits, and surface-exposure history. Lunar mare basalts typically contain about 50 volume percent pyroxene of extremely variable composition, 20-30 % Ca-rich plagioclase, 0-10 % olivine of variable composition, 0-25 % ilmenite, and 0-5% chromite-ulvöspinel solid solution. Minor amounts of troilite, Fe-metal, cristobalite or tridymite (silica polymorph), apatite or whitlockite, and K-rich glass are also generally present, usually in the mesostasis. These phases plus various impact and volcanic glasses and meteoritic minerals are present in the mare soils. The meteoritic components constitute ~ 2 % of the soil, but these minerals are largely indistinguishable because of compositions overlapping with the indigenous lunar minerals. For this study, the soil glasses have been grouped into four groups: Ti-rich glass, FeMg-rich glass, Al-rich glass, and K-rich glass. The Ti-rich glass has two origins, pyroclastic and impact melting of ilmenite-rich target material. The FeMg-rich glass has similar origins, pyroclastic and impact melting of pyroxene or olivine-rich targets. K-rich glass is derived from the mesostases of basalts or impact melting of KREEPy [*Warren and Wasson*, 1979] targets. Most mare impact glasses have a wide range of composition, but the average composition is similar to that of the bulk soil [*Hu and Taylor*, 1977]. The bulk composition of mare soils ranges of 10-15 % $Al_2O_3$. With this in mind, we termed this most abundant impact glass as Al-rich glass (10-20 weight % $Al_2O_3$).

The following phases were analyzed in the nine mare soils: ilmenite, plagioclase, olivine, pyroxene (low-Ca and high-Ca pyroxene were grouped together), Cr-Ti-spinel, troilite, Fe-metal, cristobalite (used for all silica polymorphs), Ti-rich glass, FeMg-rich glass, K-rich glass, and Al-rich glass. Phosphates were not included in the analyses owing to extremely low abundances. For reasonable counting times (40-60 ms) ilmenite ($FeTiO_3$) and ulvöspinel ($Fe_2TiO_4$) cannot be distinguished, but the generally greater abundances of the former allows all Ti-rich minerals to be called ilmenite with minimal error. All modal data are reported in Table 1.

Some general mineralogical trends are apparent. First, the amount of Al-rich glass is a strong function of $I_s$/FeO (Table 1 and Figure 2). In fact, this prominent impact-glass type increases nearly exponentially with maturity, as a function of increases in agglutinates. Conversely, the total mineral contents are lower in the more mature soils. The A-12 samples, 12001 and 12030, plot above the general trend, suggesting that they are more petrographically mature than indicated by their $I_s$/FeO values. The A-17 samples seem to have a distinct trend from the A-11 and A-15 soils. This may be due to local differences in basalt texture and composition. More likely, the A-17 trend is fortuitous, and more data may possibly indicate a broader correlation. In other words, many parameters affect soil formation, and it is not possible to account for all of them, such that simple correlations are not necessarily anticipated. The two possible origins of Ti-rich and FeMg-rich glasses provide complex trends, and this is discussed in the Petrography section below.

**Table 1.** Phase abundances of the soils (90-150 μm size fraction) characterized by this study. Data are from X-ray digital-imaging analyses and are in terms of volume percentages. $I_s$/FeO values are listed also [*Morris*, 1978].

| | 10084 | 12001 | 12030 | 15041 | 15071 | 70181 | 71061 | 71501 | 79221 |
|---|---|---|---|---|---|---|---|---|---|
| **$I_s$/FeO** | 78 | 56 | 14 | 94 | 52 | 47 | 14 | 35 | 81 |
| ilmenite | 6.0 | 0.9 | 1.7 | 0.8 | 1.8 | 7.9 | 9.8 | 12.6 | 5.8 |
| ilmenite (wt.%)[†] | 9.1 | 1.5 | 2.6 | 1.2 | 2.7 | 11.8 | 14.5 | 18.3 | 9.1 |
| Cr-spinel | 0.2 | 0.2 | 0.2 | 0.3 | 0.5 | 0.1 | 0.1 | 0.2 | 0.1 |
| plagioclase | 15.8 | 12.3 | 14.9 | 16.2 | 21.9 | 15.7 | 19.1 | 15.9 | 17.1 |
| plagioclase (wt.%)[†] | 13.9 | 11.2 | 13.4 | 14.9 | 19.9 | 13.7 | 16.4 | 13.5 | 15.6 |
| pyroxene | 32.6 | 31.1 | 43.2 | 28.1 | 38.2 | 34.0 | 34.6 | 38.5 | 21.8 |
| olivine | 1.9 | 8.8 | 6.5 | 5.5 | 4.5 | 2.9 | 3.5 | 3.4 | 3.1 |
| cristobalite | 0.3 | 0.3 | 0.3 | 0.3 | 1.8 | 0.2 | 0.7 | 0.5 | 1.2 |
| Fe-metal | tr[§] | tr | tr | tr | tr | tr | 0.4 | tr | tr |
| troilite | 0.1 | 0.1 | 0.1 | 0.1 | tr | tr | 0.2 | tr | tr |
| K-rich glass | 1.0 | 1.5 | 1.7 | 1.6 | 0.9 | 0.5 | 0.7 | 0.5 | 0.8 |
| Ti-rich glass | 7.9 | 1.4 | 1.4 | 0.6 | 0.6 | 11.3 | 13.2 | 7.7 | 8.4 |
| FeMg-rich glass | 6.5 | 7.8 | 7.8 | 12.0 | 12.9 | 2.7 | 2.5 | 2.8 | 2.6 |
| Al-rich glass | 27.6 | 37.3 | 23.2 | 35.6 | 19.6 | 25.1 | 15.6 | 18.3 | 39.3 |
| Total | 99.9 | 99.9 | 99.9 | 100 | 99.9 | 99.9 | 99.8 | 99.8 | 99.8 |

[†]Weight percentage data calculated with appropriate specific gravity values.
[§]tr = trace; < 0.1 %

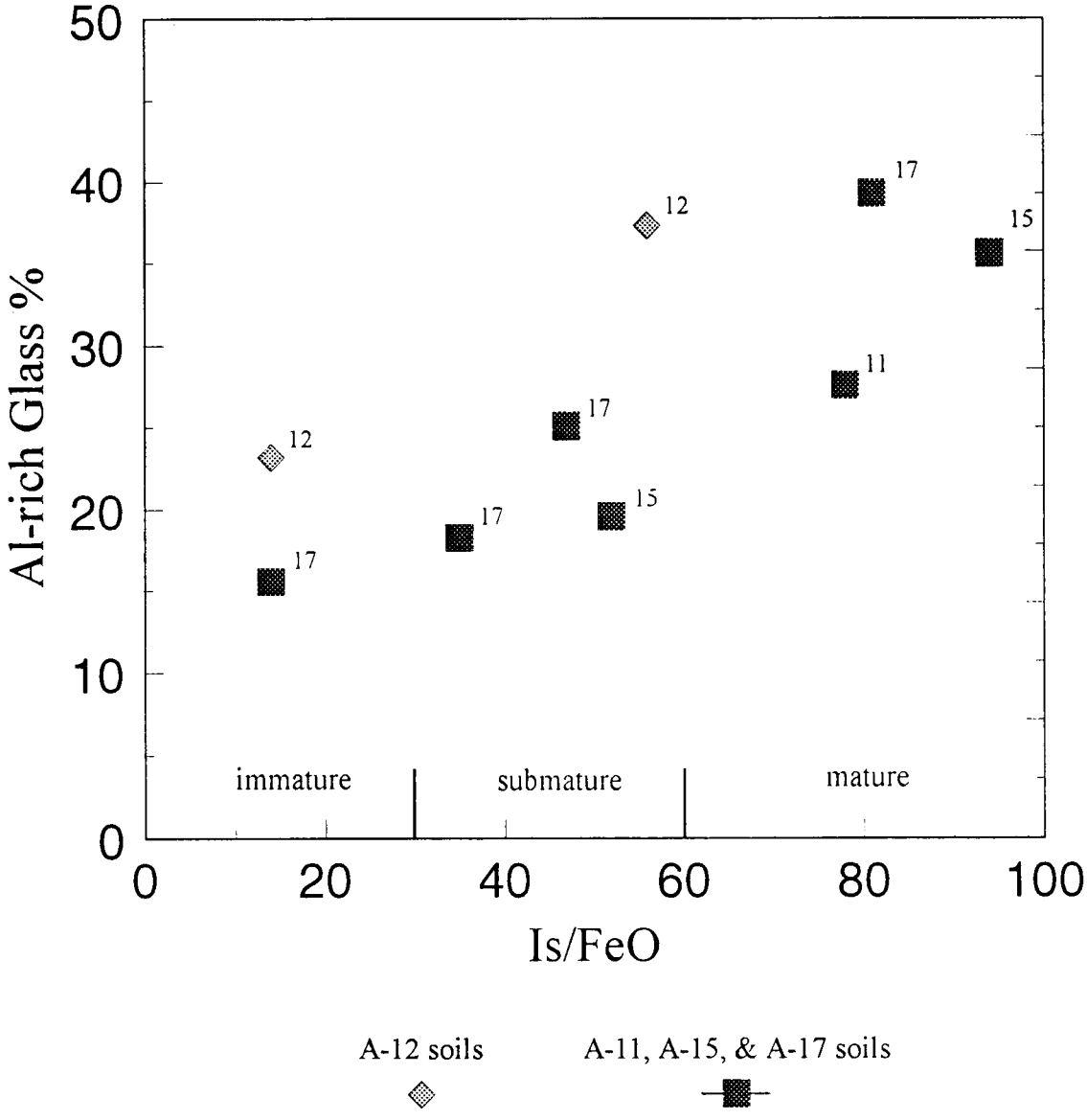



**Figure 2.** Variation of Al-rich glass (impact glass) content of mare soils versus Is/FeO [*Morris*, 1978]. The Al-rich glass percentage of the A-11, A-15, and A-17 soils studied herein increases exponentially with Is/FeO (maturity index). Glass abundance data are from Table 1. Sample mission numbers are places next to each point.

As noted above, impact melting of lunar material results in lower modal mineral content, but the normative mineralogy ("norm"), as calculated from bulk chemistry and mineral formulae, remains nearly constant. Norms and modes are quite similar for holocrystalline mare basalts, especially for minerals with limited variance from ideal composition (*e.g.*, ilmenite and plagioclase). This is not the case for mature lunar soils as the normative/modal ratio increases, because of impact melting associated with surface exposure (*i.e.*, minerals go into the melt phase). Figure 3 shows the close correspondence of norms and modes for basalts, and the general divergence of these parameters during soil maturation, in terms of $I_s$/FeO values. The norm/mode ratio increases linearly for ilmenite and logarithmically for plagioclase. In fact, the $r^2$ value for the ilmenite data (not including the A-12 points and point with the highest $I_s$/FeO value, from A-15) is 0.72, and the $r^2$ value for the plagioclase data (not including A-12 data) is 0.90. The different relationships may be due to the enhanced fusion of the < 10 μm portion of the soil which is enriched in plagioclase, followed by addition of exotic plagioclase from highland soils. This scenario would explain the large initial rise of the normative/modal plagioclase ratio and subsequent flattening with increasing $I_s$/FeO. As with the Al-rich glass versus $I_s$/FeO trend, the A-12 soils appear more mature in terms of the normative/modal ratio as compared to the ferromagnetic maturity parameter.

Phase volume percentage data can be converted to weight percentages using the appropriate specific gravity values. Weight percentage modes of ilmenite and plagioclase are reported in Table 1 for comparison with the volume data. It is clear that the high specific gravity of ilmenite (~ 4.7) as compared to the silicates (2.65-3.25),

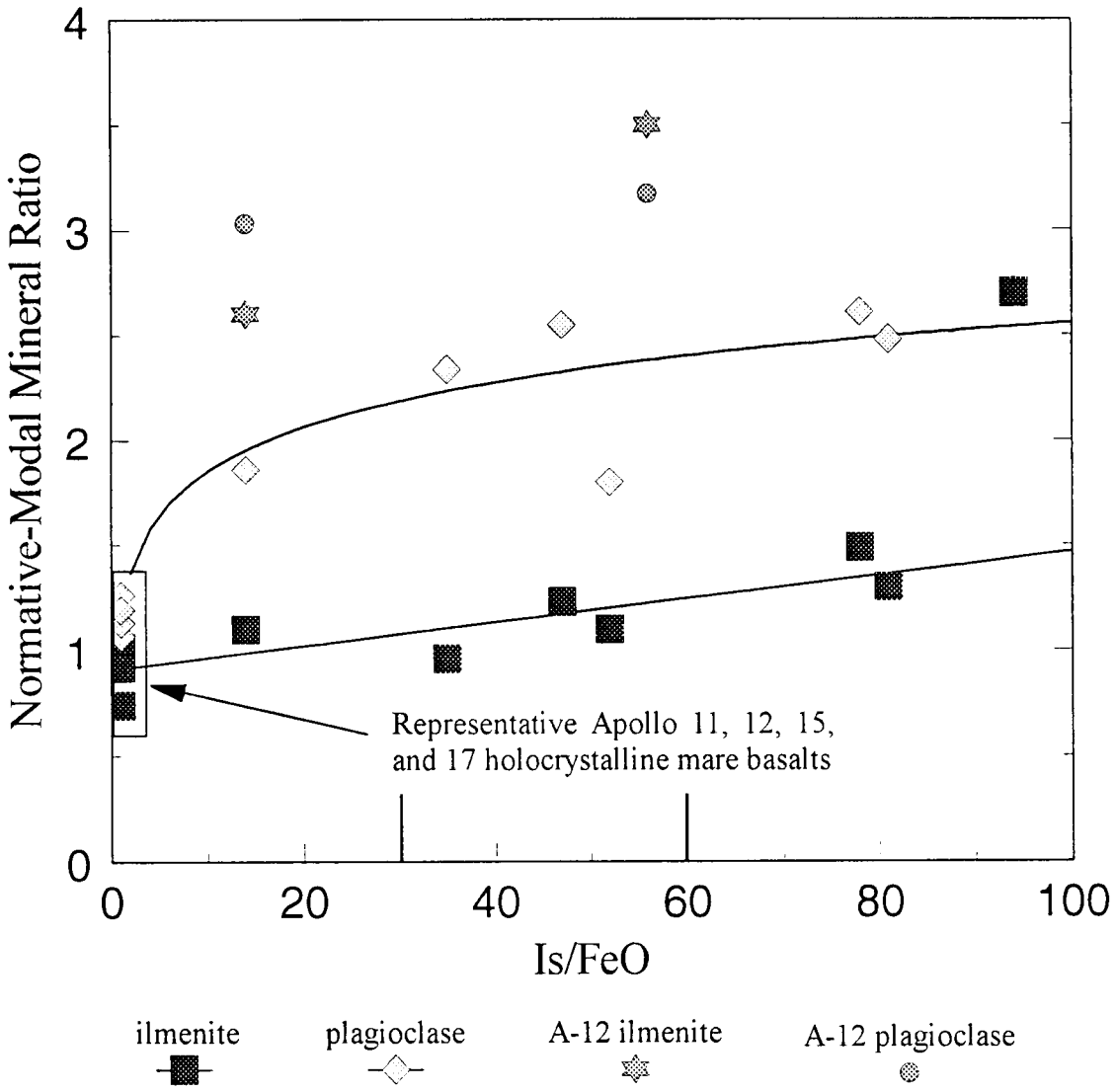



**Figure 3**. Variation of the normative/modal ilmenite ratios of mare soils of varying maturity. Is/FeO values are from *Morris* [1978]. Normative values are calculated by assigning An=90 for plagioclase and assuming ideal stoichiometry for ilmenite. Based upon An contents of plagioclase in basalts from each Apollo site [*Heiken et al.* eds., 1991], the average An content of plagioclase in the soil is judged to be 90 +/- 5 %. Basalts are arbitrarily assigned Is/FeO = 1, and they are plotted to illustrate the close agreement between normative and modal mineralogy of plagioclase and ilmenite for holocrystalline mare basalts. Soil modal data are from this study (Table 1). Ilmenite norms of A-11/A-17 soils were calculated by correcting titanium content due to pyroclastic glass.

provides for a dramatic increase upon the volume to weight percentage conversion. This has important applications for mineral-resource evaluation, as weight-based modes are needed to calculate various predicted extraction yields (*e.g.*, oxygen liberation from ilmenite).

## Petrography

The lunar soils contain a great number of particle types ranging from simple, clean-mineral fragments to complex, multiphase agglutinates and breccia, to glass beads of pyroclastic and impact origin. Classification of these entities is subjective. Some investigators use as few as 5 or 6 classes while others utilize 30-40 classes. Nevertheless, all indigenous lunar soil particles can be broadly subdivided into four main classes: free or clean mineral fragments, lithic fragments, fused-soil particles, and pyroclastic glass beads and fragments. Obviously, mineral fragments include any clean minerals derived from the local bedrock and boulders or ballistic transport from other locations. Lithic fragments in mare soils are generally basalt (multimineralic) clasts, although some highland rock fragments are possibly present. For this study, fused-soil particles were divided in four subclasses: melt glass (80-100 % glass), agglutinates (a mixture of minerals and Al-rich and FeMg-rich glass with vesicles), breccia (a mixture of minerals and Al-rich and FeMg-rich glass without vesicles) and melt rocks (high Al-rich and FeMg-rich glass content, low mineral content, and no vesicles). Breccia and melt rocks are probably equivalent to low- and high-grade (or dark matrix) breccia, respectively, of previous studies [*e.g., Heiken and McKay*, 1974]. Table 2 contains the

particle-count data in terms of volume percentages for mare soils of this study. The optical-microscopic, particle-count agglutinate data from the literature are also provided. These data, from previous work, are from many different size fractions (not just the 90-150 μm), but they are generally similar to the digitally-derived agglutinate data. There is considerable discrepancy between this study's and previously published agglutinate content of soil 12030. *McKay et al.* [1971] determined that 12030 contained only 0.5 % agglutinates, as compared to 30.9 % agglutinates by this study. Their analysis used the 250-1000 μm size fraction, as compared to the 90-150 μm size fraction used by this study, and this is apparently the reason for the large difference in estimated agglutinate abundance.

The data in Table 2 show that agglutinate percentages increase and basalt fragments decrease with maturity ($I_s$/FeO). The total abundance of free mineral fragments is a complex function of maturity, but they are generally less in mature soils. These trends are shown on a "Taylor and McKay-1992" style plot in Figure 4. Indeed, the trends generalized by Figure 1 are apparently present, although not as smooth. This is probably because of variations of the compositions and textures of basalts from which these soils were derived. Again, A-12 samples appear to exhibit a dichotomy with respect to petrographic agglutinate percent and $I_s$/FeO values.

The distribution of pyroclastic glasses (Table 2) explains the complex abundance patterns of Ti-rich and FeMg-rich glass. Essentially, the concentrations of Ti-rich and FeMg-rich glass are largely governed by the availability of local and regional

**Table 2.** Particle petrography of the soils (90-150 μm size fraction) characterized by this study. Data are from digital-imaging analyses and are in terms of volume percentages. $I_s$/FeO values are listed also [*Morris*, 1978].

| | 10084 | 12001 | 12031 | 15041 | 15071 | 70181 | 71061 | 71501 | 79221 |
|---|---|---|---|---|---|---|---|---|---|
| **$I_s$/FeO** | 78 | 56 | 14 | 94 | 52 | 47 | 14 | 35 | 81 |
| **Mineral Fragments** | | | | | | | | | |
| ilmenite | 0.9 | 0.1 | 0.1 | 0.3 | 1.0 | 3.5 | 4.1 | 5.6 | 1.9 |
| plagioclase | 5.2 | 3.9 | 3.9 | 6.5 | 12.9 | 8.9 | 9.5 | 6.9 | 5.6 |
| olivine | 0.7 | 4.2 | 2.9 | 3.0 | 2.6 | 0.1 | 0.3 | 0.5 | - |
| pyroxene | 15.2 | 13.3 | 23.3 | 13.2 | 25.1 | 16.9 | 16.9 | 16.6 | 7.5 |
| **Lithic Fragments** | | | | | | | | | |
| basalt | 18.6 | 9.3 | 21.9 | 9.6 | 16.4 | 14.4 | 26.8 | 26.3 | 12.5 |
| **Fused Soil Particles** | | | | | | | | | |
| melt glass | 2.5 | 5.5 | 5.4 | 5.6 | 2.2 | 1.3 | 1.1 | 0.7 | 5.2 |
| breccia | 5.9 | 5.3 | 7.4 | 5.3 | 3.1 | 3.7 | 5.8 | 4.6 | 5.0 |
| melt rocks | 3.3 | 3.7 | 4.1 | 3.2 | 2.7 | 3.6 | 5.1 | 2.5 | 6.9 |
| agglutinates | 45.9 | 54.8 | 30.9 | 52.6 | 31.9 | 38.4 | 14.8 | 31.8 | 51.0 |
| agglutinates[†] | 52 | 40 | 0.5 | 40 | 35 | 56 | 9 | 35 | 44 |
| **Pyroclastic Glass** | | | | | | | | | |
| orange glass | 1.5 | - | - | - | - | 4.2 | 4.8 | 1.3 | 1.9 |
| black glass | 2.4 | - | - | - | - | 4.9 | 9.8 | 2.9 | 2.4 |
| green/yellow glass | - | - | - | 0.7 | 1.8 | - | - | - | - |
| # particles | 940 | 705 | 990 | 787 | 818 | 452 | 514 | 584 | 839 |

[†]Agglutinate particle counts of various size fractions of these soils by various workers. Data taken from the Handbook of Lunar Soils [compiled *Morris et al.*, 1983].

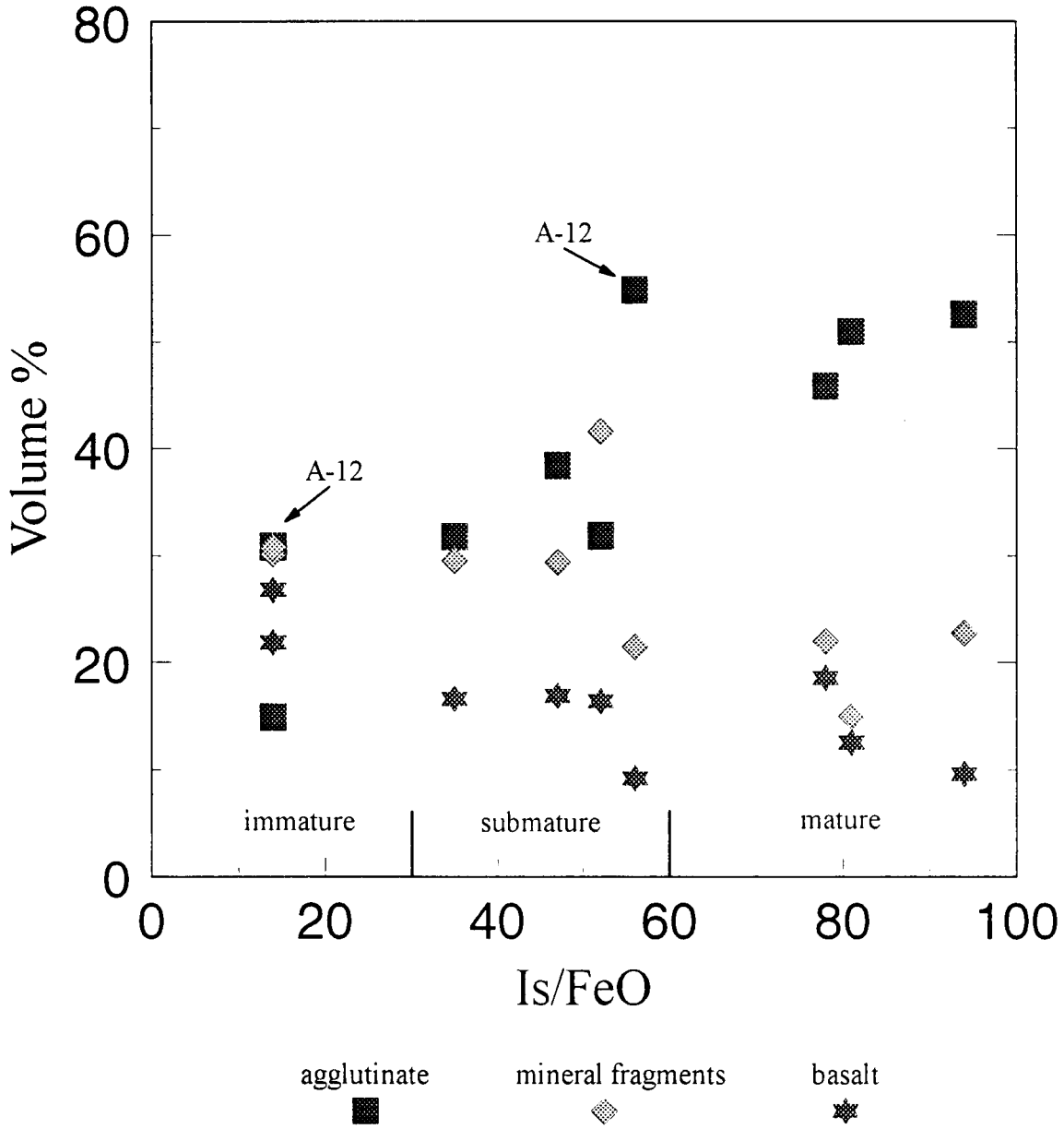



**Figure 4**. Petrographic development of mare soils. Particle-type volume % data are from Table 2. The trends are similar to those predicted by *Taylor and McKay* [1992]. Note that the A-12 samples have agglutinate % above the general trend.

pyroclastic deposits. For instance, the A-11 and A-17 soils are enriched in Ti-rich glass, not because of impact melting of ilmenite but to mixing with local pyroclastic deposits (*e.g.*, soil 72440 from Shorty Crater). A similar scenario explains the enrichment of FeMg-rich glass in soils 15041 and 15071. Impact processes act mainly to redistribute these materials within the more voluminous gray mare soils. As such, no strong trends in the absolute abundance of Ti-rich and FeMg-rich glasses are apparent with $I_s$/FeO values (Table 1).

As noted, the data in Table 2 are in terms of volume percentages, as determined by digitizing of each grain. Optical particle-count data are reported as volume percentages, because of the tacit assumption that particle percent is equivalent to volume percent. This is strictly true only if all the particles in a grain mount are the same size. The small size-fraction interval (90-150 μm) analyzed by this study provided for nearly 1:1 correspondence between particle and volume data, and therefore, only the latter are reported. This will probably not be the case for large size-fraction ranges (*e.g.*, 90-1000 μm).

## Modal Data versus Particle Counts

As discussed in the introduction, optical particle counts have been wrongly referred to as modal analyses. This has suggested that high-Ti mare soils are greatly depleted in ilmenite, as compared to high-Ti basalts [*e.g., Heiken and Vaniman*, 1990]. Comparison of true modal data (Table 1) and particle-count data (Table 2) shows that all mineral concentrations are underestimated by factors of 2-17 if one assumes particle

percent represents mineral modal percent. Figure 5 displays this observation for ilmenite, plagioclase, and pyroxene. This point is vital for mineral resource evaluation of lunar soils and for appreciating soil mineralogy in general. Since spectral reflectance studies use particle-count data for calibration, soil mineral composition estimated by this method only provides particle percentages not actual modes. As such, recalibration with modal data is warranted. To a first approximation, it may be possible to adjust the particle-count mineralogy to modal mineralogy by multiplying by a factor of two to three, as estimated from Figure 5.

## Petrographical Maturity versus Magnetic Maturity Parameters

Lunar soil is a complex material, and simple smooth trends are not necessarily expected with respect to the various maturity parameters. Nevertheless, some trends are apparent: agglutinate %, Al-rich glass (impact) %, and the normative/modal ratio all increase with $I_s$/FeO (Figures 2, 3, and 4, respectively). The A-12 soils, 12001 and 12030, appear petrographically more mature than indicated by their $I_s$/FeO data for all these general trends.

The correlation between petrographic agglutinate and $I_s$/FeO was discussed by *Morris* [1976]. Since all $I_s$/FeO data were generated by *Morris* [1976, 1978], interlaboratory bias is not a concern for this parameter. The petrographic agglutinate data discussed by *Morris* [1976] come from similar sources [*Heiken et al.*, 1973; *McKay et al.*, 1974, *McKay and Heiken*, 1973; *D.S. McKay*, unpublished results], and therefore, not much interlaboratory bias is anticipated here also. It is important to note that the

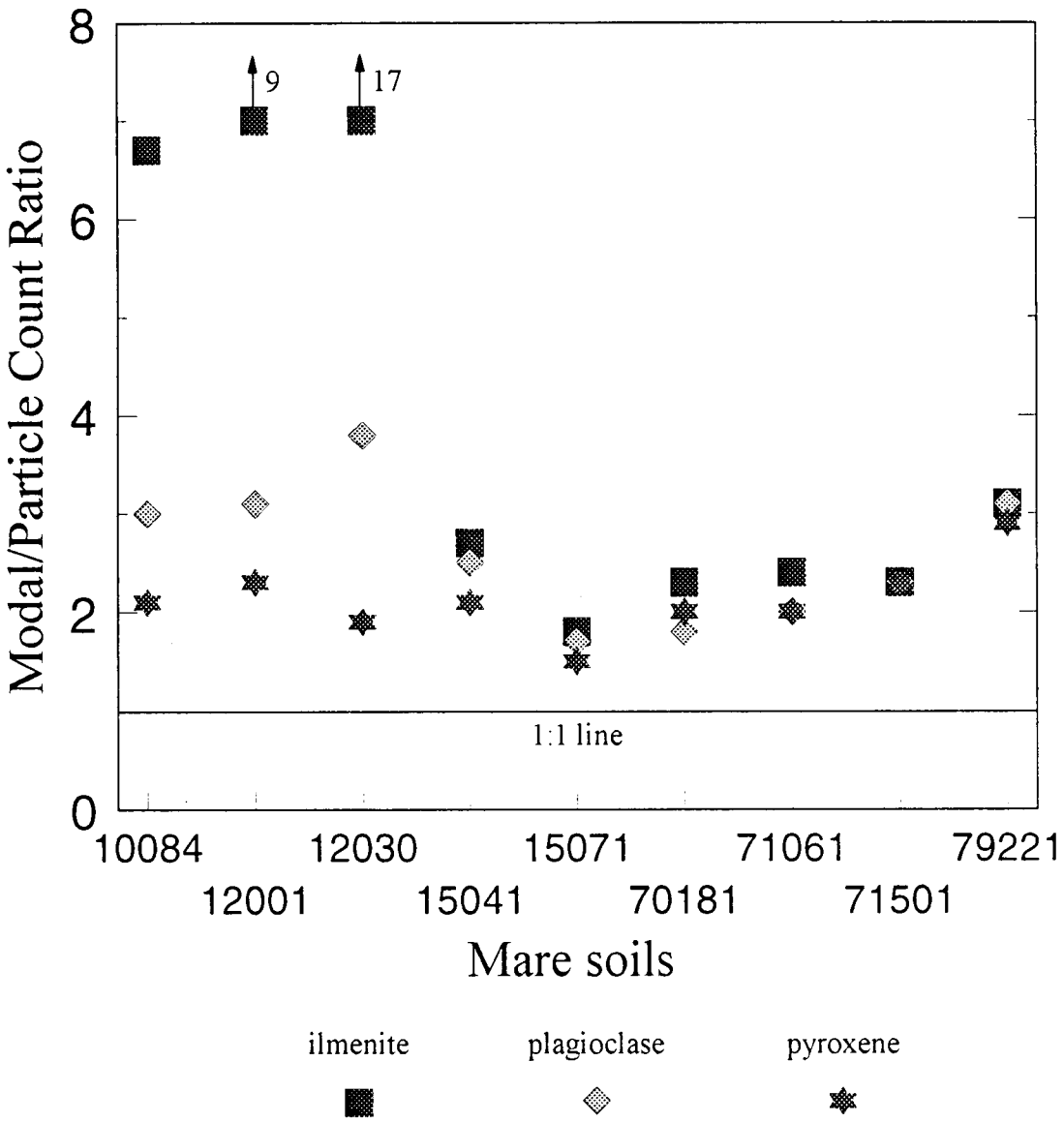



**Figure 5.** Ratio of modal mineral abundance (volume %) to particle count data (volume %). Data are from this study and are reported in Tables 1 and 2. Note the lack of 1:1 correspondence between the modal data and particle-count data.

overall positive correlation displayed in *Morris* [1976] for lunar soils does not include data for A-11 and A-12 soils, although both are listed in the figure key (see Figure 4 in *Morris*, 1976]. Apparently, this was because of the absence of data for the 90-150 μm fractions of these soils, as petrographic agglutinate data are not listed in Table 1 of *Morris* [1976] either.

In order to compare the data of the A-12 soils to the general agglutinate versus $I_s$/FeO trend of other mare soils (only A-15 and A-17), the data compilation of *Morris* [1976] is plotted in Figure 6. The data field is broad, much broader that the near linear trend ($r^2 = 0.93$, not including A-12 samples) for data of the present study. This could be attributed to some interstudy bias for the agglutinate data or to the fact that the field data are composed of 71 points as compared with 7 for this work. Nevertheless, the $I_s$/FeO and geographic ranges of the data base in Table 2 are large. It is noteworthy that A-12 soil 12030 plots above the general trend of the A-11, A-15, and A-17 soils. Sample 12001 plots within the field but at the upper portion. In conclusion, the A-12 soils 12001 and 12030 appear somewhat more petrographically mature than other mare soils with comparable $I_s$/FeO values, as evidenced by Figures 2-6.

Examination of the various mare soil-sample locations may explain the A-12 soil data. Craters are an ubiquitous feature of the lunar surface at all Apollo landing and sampling sites. Nevertheless, the cratering density of the Moon is not necessarily uniform (*e.g.*, there are many more large near-side basins of Nectarin and Imbrium age). Sampling site maps are provided in The Handbook of Lunar Soils [*Morris et al.*, 1983].

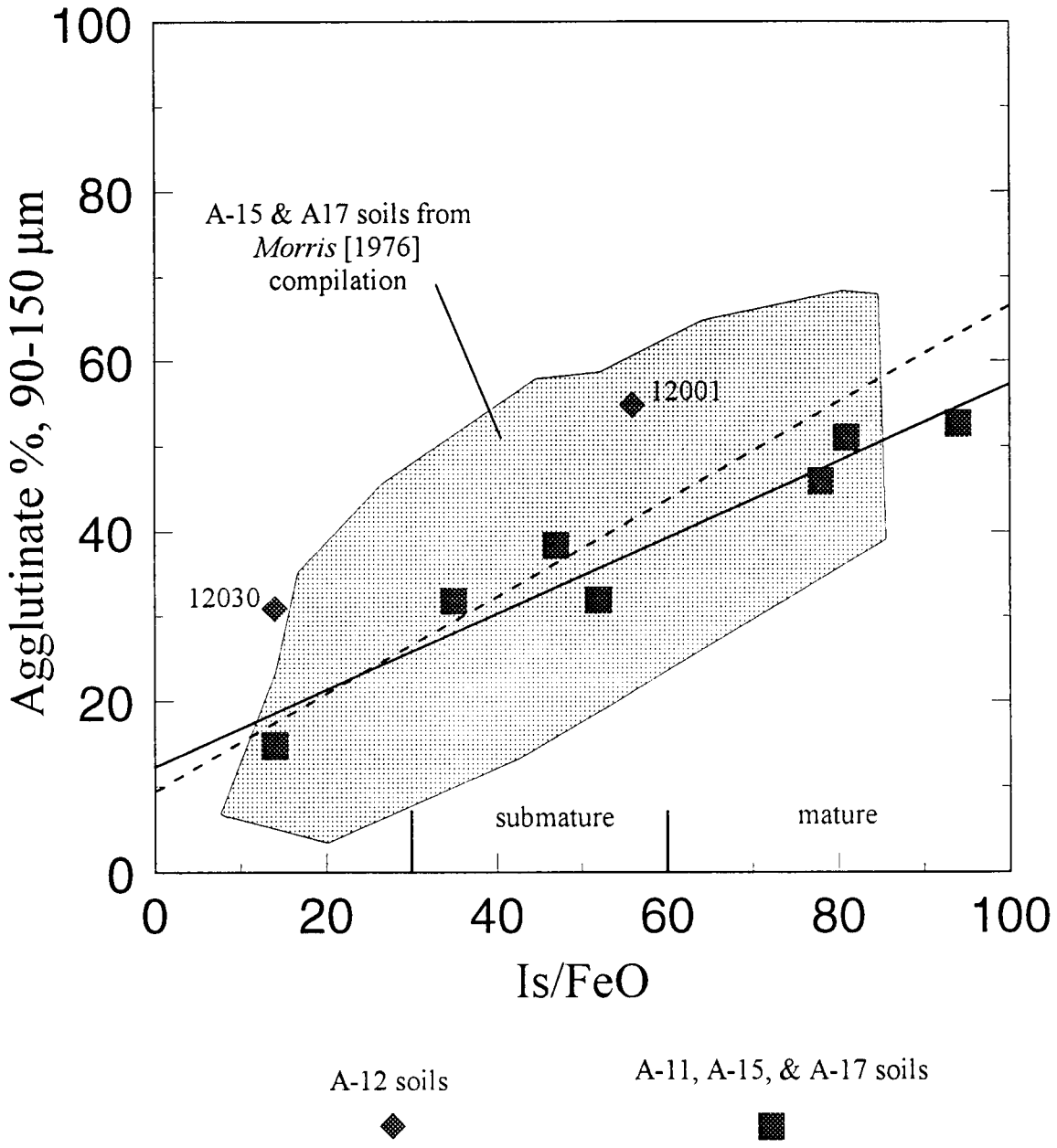



**Figure 6.** Comparison of petrographic agglutinates versus Is/FeO data of mare soils (A-15 and A-17) from *Morris* [1976] compilation and data from this study. Note that the general trend is broad. The dashed line represents the linear regression of the "field" data. The A-12 samples plot near the top extent of the general trend.

Evaluation of these maps indicates that several 100 meter-scale impact craters are present at the A-12 site, namely Bench, Head, and Surveyor.

Close proximity of larger scale impacts can effectively increase the amount impact glass without strongly affecting the $I_s$/FeO values, provided that the melted target material consisted of young soil or bedrock and boulders. In other words, these materials do not possess much reducing solar-wind hydrogen and carbon. It appears (from evaluation of sampling maps) that the local 100 meter-scale crater density of the A-12 site is somewhat higher than that of A-11, A-15, and A-17 sites. In effect, the petrographic maturity of A-12 soils may be overprinted by the addition of impact glass from these larger-scale events. This hypothesis is supported by the fact that two 4-cm agglutinates, very large by comparison to typical agglutinates (usually < 1mm, *Heiken et al.*, eds. 1991), were collected with 12030, and several glass (impact ?) beads were noted during the collection of soil 12001. Furthermore, optical petrography during this study noted a significantly greater amount of spherical agglutinates in 12001 as compared to the other soils. These spherical agglutinates were likely formed in flight as semi-molten blobs of silicate melt and mineral fragments because of larger-scale impact events, as compared to being formed on the soil surface by small-scale quiescent events responsible for the more abundant irregularly shaped agglutinates.

These observations may not be limited to the A-12 site. In fact, the general petrographic agglutinate versus $I_s$/FeO trends of mare soils may be largely the result of only A-15 and A-17 soils being included in the data interpretation. Local geology and impact history may impart a stronger control on some lunar soils, such as A-12 samples.

With this in mind, digital-image analyses of additional A-12 soils are warranted. More importantly, further lunar soil sampling may be required before extrapolating trends to the rest of the Moon and other planetary bodies.

## SUMMARY

True modal analyses performed by X-ray digital-imaging of mare soils from Apollo 11, 12, 15, and 17 sites demonstrate that optical particle-count data are inadequate for estimating actual mineral abundances. This is significant as true modal data are required for mineral resource evaluation, and this type of data will enhance petrologic understanding of lunar soils, paramount for remote sensing studies.

Impact melting of the primary basaltic minerals and auto-reduction produce some notable soil maturation trends. Al-rich glass (*i.e.*, impact or agglutinitic) increases nearly exponentially with the ferromagnetic index, $I_s$/FeO. Impact melting causes a divergence of the normative and modal mineralogy with increased surface exposure. This is manifested as a marked increase in the normative/modal ratio of ilmenite and plagioclase (and presumably other minerals) with $I_s$/FeO. Therefore, modal analyses are required to estimate soil mineral content, as normative calculations do not take into account the transformation of minerals to impact glass.

Petrographic data (*i.e.*, particle counts) of nine mare soils shows a general increase of agglutinates and decrease of basalt fragments with maturation. Mineral liberation is more complex because of the competing processes of comminution and agglutination. The abundance of free mineral fragments is greater for immature and

submature soils and lower for the mature soils of this study. Ideal agglutinate-basalt-mineral fragment evolution curves of *Taylor and McKay* [1992] are generally followed by the mare soils analyzed during this work.

The two A-12 soils consistently plotted off the petrographic-magnetic maturity parameter trends of the other seven soils. Basically, 12001 and 12030 appear petrographically more mature than indicated by their respective $I_s$/FeO values, at least comparing with A-15 and A-17 soils. Evaluation of *Morris* [1976] indicates that A-12 soils were not included in the familiar agglutinate versus $I_s$/FeO plot, apparently because of the lack of petrographic data for the 90-150 μm size fractions. Inclusion of these two data points shows that 12030 plots outside the general trend. 12001 plots within the "Morris" data field, but well above the regression line. The close proximity of several 100 meter-scale craters and the occurrence of unusually large and spherical agglutinates suggest that local larger-scale impact events overprinted the gradual regolith maturation process at Apollo 12. This may not be unique to A-12 soils. As such, more digital-imaging investigations of A-12 soils and further sampling are necessary for a better understanding of the complexities of soil formation on the Moon and other airless planetary bodies.

# REFERENCES


Bates, R.L. and J.A. Jackson (eds.), *Glossary of Geology* 3rd Edition, American Geological Institute, Alexandia, VA, 1987.

Chambers, J.G., L.A. Taylor, A. Patchen, and D.S. McKay, Mineral liberation and beneficiation of lunar high-Ti mare basalt, 71055: Digital-imaging analyses, in *Engineering, Construction, and Operations in Space IV*, pp. 878-888, American Society of Civil Engineers, New York, 1994a.

Chambers, J.G., A. Patchen, L.A. Taylor, S.J. Higgins, and D.S. McKay, Lunar mineral feedstocks from rocks and soil: X-ray digital-imaging in resource evaluation (abstract), *Lunar Planet. Sci. Conf. XXV*, pp. 235-236, 1994b.

Chambers, J.G., L.A. Taylor, A. Patchen, and D.S. McKay, Quantitative mineralogical characterization of lunar high-Ti mare basalts and soils of oxygen production, *submitted to JGR-Planets*, 1995.

Chambers, J.G., L.A. Taylor, A. Patchen, and D.S. McKay, True modal analyses of lunar mare soils: X-ray digital-imaging, *Lunar Planet. Sci. Conf. XXVI*, 1995.

Delano, J.W., Pristine lunar glasses: Criteria, data, and implications, *Proc. Lunar Planet. Sci. Conf. 16th*, pp. D201-D213, 1986.

Haskin, L.A. and R.L. Korotev, Test of a model for trace element partion during closed-system solidfication of a silicate liquid, *Geochim. Cosmochim. Acta*, v. 41, pp. 921-939, 1977.

Heiken, G.H., M. Duke, D.S. McKay, U.S. Clanton, R. Fryxell, J.S. Nagle, R. Scott, and G.A. Sellers, Preliminary stratigraphy of the Apollo 15 drill core, *Proc. Lunar Planet. Sci. Conf. 4th*, pp. 191-213, 1973.

Heiken, G.H. and D.S. McKay, Petrography of Apollo 17 soils, *Proc. Lunar Planet. Sci. Conf. 5th*, pp. 843-860, 1974.

Heiken, G.H. and D.T. Vaniman, Characterization of lunar ilmenite resources, *Proc. Lunar Planet. Sci. Conf. 20th*, pp. 239-247, 1990.

Heiken, G.H., D.T. Vaniman, and H. Hawkins, Sulfur as a lunar resource, in *Engineering, Construction, and Operations in Space III*, pp. 555-564, American Society of Civil Engineers, New York, 1992.

Higgins, S.J., A. Patchen, J.G. Chambers, L.A. Taylor, and D.S. McKay, Petrographic characterization of lunar soils: Application of X-ray digital-imaging to quantitative and automated analysis (abstract), *Lunar Planet. Sci. Conf. XXV*, pp. 547-548, 1994.

Higgins, S.J., J.G. Chambers, L.A. Taylor, A. Patchen, and D.S. McKay, X-ray digital-imaging petrography Part I: Technique development for lunar (mare) soils, *in press.*

Housley, R.M., R.W. Grant, and N.E. Paton, Origin and characteristics of excess Fe metal in lunar glass welded aggregates, *Proc. Lunar Planet. Sci. Conf. 4th*, pp. 2737-2749, 1973.

Housley, R.M., E.H. Cirlin, I.B. Goldberg, H. Crowe, R.A. Weeks, and R. Perhac, Ferromagnetic resonance as a method of studying the micrometeorite bombardment history of the lunar surface, *Proc. Lunar Planet. Sci. Conf 6th*, pp. 3173-3186, 1975.

Hu, H.N. and L.A. Taylor, Lack of chemical fractionation in major and minor elements during agglutinate formation, *Proc. Lunar Planet. Sci. Conf. VIII*, pp. 3645-3656, 1977.

Kramer, F.E., D.B. Twedell, and W.J.A. Walton, Jr., *Apollo 11 lunar sample information catalog* (revised), NASA-JSC, 1977.

Labotka, T.C., M.J. Kempa, C. White, J.J. Papike, and J.C. Laul, The lunar regolith: Comparative petrology of the Apollo sites, *Proc. Lunar Planet. Sci. Conf. 11th*, pp. 1285-1305, 1980.

Laul, J.C. and J.J. Papike, The lunar regolith: Comparative chemistry of the Apollo sites, *Proc. Lunar Planet Sci. Conf. 11th*, pp. 1395-1413, 1980.

Lofgren, G.R. and E.M. Lofgren, *Catalog of lunar mare basalts greater than 40 grams-Part 1: Major and Trace Chemistry*, Lunar and Planetary Contribution 438, pp. 418, 1981.

McKay, D.S., D.A. Morrison, U.S. Clanton, G.H. Ladle, and J.F. Lindsay, Apollo 12 soil and breccia, *Proc. Lunar Planet. Sci. Conf. 2nd*, pp. 755-774, 1971.

McKay, D.S. and G.H. Heiken, The South Ray Crater age paradox, *Proc. Lunar Planet. Sci. Conf. 4th*, pp. 41-47, 1973.

McKay, D.S., R.M. Fruland, and G.H. Heiken, Grain size and the evolution of lunar soils, *Proc. Lunar and Planet. Sci. Conf.* V, pp. 887-906, 1974.

Warner, J., *Apollo 12 Lunar Sample Information*, NASA Technical Report R-353, 1970.

Warren, P.H. and J.T. Wasson, The origin of KREEP, *Rev. Geophys. Space Phys.*, v.17, pp. 73-88, 1979.

# VITA

John Gregory Chambers was born in Carrollton, Georgia on May 20, 1969. He attended primary and elementary schools of Bowdon (Georgia), which was part of the Carroll County School System. His high school education was received from Central High School, a member of the Carroll County School System. Following high school graduation in June, 1987, John started college at West Georgia College, Carrollton, Georgia in March 1988. He received the degree of Bachelor of Science with a major in Geology in June, 1992. In August, 1992, he started graduate studies at the Department of Geological Sciences, the University of Tennessee, Knoxville. He received the degree of Master of Science with a major in Geology in May, 1995.